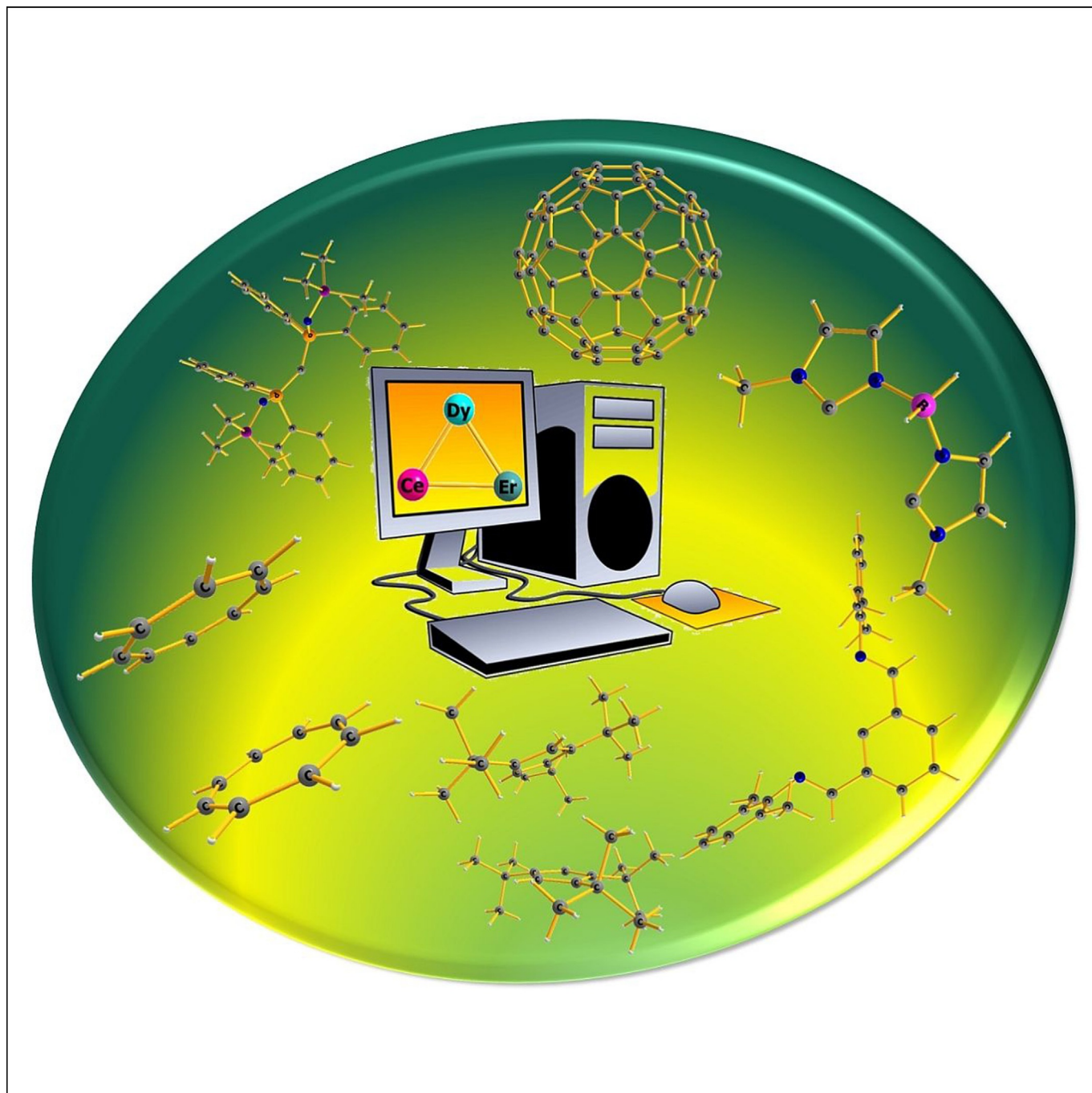


# Role of Ab Initio Calculations in the Design and Development of Organometallic Lanthanide-Based Single-Molecule Magnets

Abinash Swain, Arup Sarkar, and Gopalan Rajaraman\*<sup>[a]</sup>



**Abstract:** Single-molecule magnets based on lanthanides are very attractive due to their potential applications proposed in the area of microelectronic devices. Very recent advances in this area are due to the blend of conventional lanthanide chemistry with organometallic ligands, and several breakthrough achievements are attained with this combination. Ab initio methods based on multi-reference CASSCF calculations are playing a vital role in the design and devel-

opment of such molecules. In this minireview, we aim to appraise various contributions in the area of organometallic lanthanide complexes (those containing lanthanide-carbon bonds) and describe how these robust wavefunction-based methods have played a constructive role not only in rationalizing the observed magnetic properties but also proven to be a potential predictive tool with some selected examples.

## 1. Introduction

Molecular Magnets offer a bottom-up approach to new generation electronic devices that are expected to replace the existing technologies in the years to come.<sup>[1]</sup> The potential applications proposed for these molecules encompass a wide range, from information storage devices that can rake up storage  $10^5$  times the current drives to solid-state Q-bits in quantum computing. Very recently utilizing these molecules for spintronic devices is emerging with several groups reporting unconventional magnetic properties of such molecules on surfaces.<sup>[2]</sup> Application for information storage devices and the desired molecule that are suited for this purpose are widely studied in this area. For this application, storage at molecular levels are sought and discovery of molecules that can retain magnetization upon removal of the magnetic field has rejuvenated this area for the last two decades. These molecules are popularly known as Single-Molecule Magnets (SMMs).<sup>[3]</sup> Particularly, SMMs comprising lanthanide ions are fascinating in the rapid development of various materials for nanoscale storage devices which can be achieved by fabrication on graphene or other metallic/non-metallic surfaces.<sup>[4]</sup> Among the SMMs family, the Single Ion Magnets (SIMs) where only one paramagnetic metal ions present in the molecule are attractive as they represent the smallest size possible where the magnetic properties can still be fine-tuned at will. There are several parameters that are associated with the SIMs characteristics that classify them as the best or the worst SIMs and these are (i) effective energy barrier for magnetization reversal ( $U_{\text{eff}}$ ) which by definition takes into consideration within single-ion framework, the barrier height for relaxation of the magnetization (ii) the blocking temperature ( $T_{\text{B}}$ ) which is defined as the temperature below which the magnetization considered frozen.<sup>[5]</sup>


One of the main parameters which shape up the characteristics of an SMM is the magnetic anisotropy, which is inherently large for the 4f elements. With larger magnetic anisotropy, lanthanides are yielding superior SMM properties and this primarily arises due to the unquenched orbital moment of the  $\text{Ln}^{\text{III}}$

ion resulting in high energy barrier to cause a reversal of magnetisation after the removal of the magnetic field.<sup>[6]</sup> Combining lanthanide ions with suitable crystal field can lead to ideal electrostatic interactions which determine the anisotropic barrier between the opposite orientations  $\pm m_j$  levels.<sup>[7]</sup> More significant the splitting by the crystal field effect greater will be the magnetic blocking barrier and blocking temperature. Due to their large anisotropy and Kramers nature of the ground state, the  $\text{Dy}^{\text{III}}$  and  $\text{Er}^{\text{III}}$  ions are considered prolific among lanthanides to yield superior SIMs. Beyond these two lanthanide ions  $\text{Tb}^{\text{III}}$ ,  $\text{Ho}^{\text{III}}$ ,  $\text{Ce}^{\text{III}}$ ,  $\text{Tm}^{\text{III}}$ , and  $\text{Yb}^{\text{III}}$  ions also reported possessing attractive blocking temperature—albeit small in numbers.<sup>[3c,8]</sup> Despite all the positive side of the lanthanides ions, the quantum tunneling of magnetisation (QTM), Raman and/or Orbach processes are still persistent, reducing significantly the blocking temperature observed for the SIMs.<sup>[9]</sup>

Apart from the nature of the lanthanide ions and its associated spin-orbit states, geometry around the metal ion which are dictated by the ligand design governs the nature of  $m_j$  level splitting and hence the magnetisation barrier. The most prolific ligand in this regard came out in 2010, after which a trend has been set to explore the SMM behaviour of organometallic based complexes.<sup>[10]</sup> The most recently discovered  $[(\text{Cp}^{\text{Pr}5})\text{Dy}(\text{Cp}^*)]^+$  and  $[\text{Dy}(\text{Cp}^{\text{ttt}})_2]^+$  ( $\text{Cp}^*$  = pentamethylcyclopentadienyl,  $\text{Cp}^{\text{Pr}5}$  = penta-isopropylcyclopentadienyl,  $\text{Cp}^{\text{ttt}}$  = 1,2,4-tri-*tert*-butylcyclopentadienyl) complexes which are found to show magnetic hysteresis opening up to 80 K and 60 K respectively, give a new ray of light in this area and pave the way forward for SMMs to be used in various devices.<sup>[11,12]</sup>

Understanding the magnetic properties of lanthanides are challenging due to the close-lying energy levels called Stark levels, which render the interpretation of experimental data often cumbersome. Several molecules reported recently with attractive magnetic properties are known earlier, but their magnetic properties have been hardly explored,<sup>[13]</sup> thanks to strong anisotropy rendering most of the routine magnetic characterisation ineffective. A significant advancement in terms of interpretation and design in lanthanide SIMs arise due to the quantum chemical calculations aided by the robust development in computing hardware, enabling one to perform high-level ab initio calculations on these molecules. Pioneering work by Chibotaru and co-workers on the development of pseudospin Hamiltonian formalism and utilisation of the same to derive useful quantities such as crystal field splitting and the corresponding g-anisotropy of lanthanide ions have trans-

[a] A. Swain, A. Sarkar, Prof. G. Rajaraman  
Department of Chemistry, Indian Institute of Technology Bombay  
Powai, Mumbai 400076 (India)  
E-mail: rajaraman@chem.iitb.ac.in

 The ORCID identification number(s) for the author(s) of this article can be found under:  
<https://doi.org/10.1002/asia.201900828>.

formed this area in the last decade.<sup>[14]</sup> These calculations are now not only aid in interpreting the experimental observations; they are also proven to be a predictive tool. Further, from the calculations of the ground and excited state wave functions, the magnetic moment for these states could be derived which later on implemented on SINGLE-ANISO routine to obtain qualitative relaxation mechanism of magnetisation reversal which has been widely used to date.<sup>[15]</sup> The approach of the crystal field towards the metal ion is rationalised by obtaining the crystal field parameter by using Steven's operator model, which shows the axial or equatorial behaviour of the crystal field.<sup>[16]</sup> It would not be an exaggeration to state that these fine understandings of the relaxation mechanism helped in the development of cyclopentadienyl ring based Dy<sup>III</sup> SIMs which are reported to possess blocking temperature crossing liquid nitrogen temperatures.<sup>[10c,17]</sup> Also, important to state here that there are many attempts to correlate the experimental findings to the computed parameters. Particularly Slageren and co-workers utilized infrared and Inelastic Neutron Scattering techniques to obtain crystal-field splitting parameter for [LnPc<sub>2</sub>]<sup>-</sup> (here Ln=Dy, Ho, Er) molecules and these were then mapped to those obtained from ab initio CASSCF calculations and excellent agreement between these two sets of numbers was found offering confidence on the obtained parameters.<sup>[18]</sup>

While several reviews on lanthanide-based SMMs and SIMs have been written earlier, here we intend to showcase the role of ab initio calculations in the design and development of organo-lanthanide SIMs.<sup>[17,19]</sup> As the Dy<sup>III</sup>/Er<sup>III</sup>-carbon bond seems to offer the most robust crystal field strength among others studied, such minireview focusing on these examples expected to gain a deeper understanding on the role of ligands and substituents on the ligand that is expected to play a critical role in the mechanism of magnetisation relaxation. To keep the review short, we have focused on selective examples of monomeric organolanthanide molecules where extensive ab initio calculations have been utilised to gain a deep understanding of the relaxation processes.

## 2.1. Choosing the right lanthanide ion for right crystal field

To design molecular magnets with substantial energy barrier for magnetic reversal requires a very high anisotropy and this makes lanthanide the most potential candidate over transition metal ions.<sup>[3c]</sup> The first lanthanide-based SIM was reported in 2003 by Ishikawa and co-workers with the discovery of slow relaxation of magnetisation in [Tb<sup>III</sup>(pc)<sub>2</sub>] (pc=phthalocyanin) promoted the focus on lanthanide-based SIMs with the primary emphasis being on the utilization of polytopic ligands to design SIMs which exhibit slow magnetic relaxation.<sup>[6]</sup> The magnetic properties of the Ln<sup>III</sup> ions strongly depend on the ground state multiplet, which is strongly coupled between the spin (S) and orbital angular (L) momenta term. The large unquenched spin-orbit coupling due to the buried 4f electron causes a large anisotropy leading to enhanced blocking barrier if a suitable ligand design present. In lanthanides, the nature of the m<sub>J</sub> ground state and the associated crystal field splitting are similar to the ground state S value and zero-field splitting

parameters of a transition metal ion SMMs. In SIMs, the m<sub>J</sub> levels are fixed, and therefore, one has to play around the crystal field parameters to enhance the magnetic anisotropy. Since large m<sub>J</sub> state is desired, naturally lanthanide ions having more than half-filled 4f orbitals are desired. In this instance, Ho<sup>III</sup>, Dy<sup>III</sup>, Er<sup>III</sup>, and Tb<sup>III</sup> are attractive as they could possess ground state as <sup>5</sup>I<sub>6</sub>, <sup>6</sup>H<sub>15/2</sub>, <sup>4</sup>I<sub>15/2</sub>, and <sup>7</sup>F<sub>6</sub> as their ground state, respectively (see Figure 1 a). While the electronic structure of the Ln<sup>III</sup> ions ensures L+S as the ground state for these ions, further splitting of these levels by crystal field dictate the nature of the anisotropy as shown in Figure 1 a.<sup>[7]</sup> Long et al. beautifully describes the nature of the electron density of the individual m<sub>J</sub> levels arise due to crystal field splitting for various 4f ions and classify them as an oblate and prolate type and suggest

*Gopalan Rajaraman (born in Thanjavur, India) received his Ph.D. at the University of Manchester, UK under the supervision of Prof. R. E. P. Winpenny and Prof. E. J. L. McInnes in 2004. He then undertook postdoctoral stays at the University of Heidelberg, Germany (2005–2007) in the group of Prof. P. Comba and the University of Florence, Italy in the group of Prof. D. Gatteschi (2007–2009). In December 2009, he joined IIT Bombay, India as an assistant professor and became a professor in 2018. His research focuses on employing electronic structure methods to understand the structure, properties and reactivity of molecules possessing unpaired electrons (open-shell systems). In addition to modelling molecular magnets, his group also actively pursue research in the area of modelling bio-mimic reactions catalysed by high-valent metal-oxo/imido complexes.*



*Abinash Swain was born in Bargarh (Odisha), India and received a B.Sc. in Chemistry from BJB College, Utkal University, Bhubaneswar in 2013. He obtained his M.Sc. from School of Chemistry, University of Hyderabad in 2015 and received UGC-JRF scholarships to undertake a Ph.D. under the supervision of Prof. Gopalan Rajaraman at IIT Bombay, India. His research interests focus on the modelling of molecular nanomagnets, with special emphasis on modelling and synthesis of Single-Molecule Toroids and analysing the ferrotoroidic behaviour of lanthanide metal complexes using DFT and ab initio calculations.*



*Arup Sarkar, born in Kolkata, West Bengal, India, completed his bachelor's degree in Chemistry from Seth Anandram Jaipuria College, Kolkata in 2012. He obtained his Master's degree with a specialisation in Inorganic Chemistry from University of Calcutta (Rajabazar Science College, Kolkata) in 2014 and then he moved to Indian Institute of Technology Bombay, Mumbai in 2015 and joined Ph.D. under Prof. Gopalan Rajaraman. He is currently a CSIR-SRF fellow, and his research interest covers the area of investigation of magnetic anisotropy in single-ion magnets containing transition metal or lanthanide complexes with the help of ab initio and DFT techniques.*





i.e., CAS( $n$ , 7) active space were chosen to optimise the orbitals to give reliable results. Apart from this, the major source of spin-orbit coupling (SOC) here is central lanthanide ion compared to the surrounding ligand atoms which contribute poorly to the overall SOC of the complex. Therefore, it is justified to use state-averaged CASSCF methodology followed by state interaction-spin-orbit interaction (SI-SO) to gain insight into the electronic structure of the lanthanide the SMMs/SIMs.<sup>[22]</sup> These final wavefunction obtained from the RASSI-SO calculations are then subjected to SINGLE ANISO routine which allows non-perturbative calculations of pseudo-spin Hamiltonians to extract various spin Hamiltonian parameters. Here the pseudospin corresponds to a Kramers doublet which is degenerate in the absence of magnetic field. Therefore the wavefunction arising from these two doublets are already eigenfunctions of the pseudo-spin  $\tilde{S} = \frac{1}{2}$  in z-projection with their orientation coincide with respect to the applied magnetic field.

The crystal field term is more appropriate for the Ln<sup>III</sup> complexes and has been developed based on metal-ligand electrostatic models. It works very well with the lanthanide complexes as 4f orbitals do not directly overlap with the ligand orbitals. Crystal field operators operate on the spin-orbit coupled states, i.e., upon the  $|J, m_J\rangle$  basis. The earlier definition of the crystal field potential  $V$  expressed in terms of Stevens operator form:<sup>[23]</sup>

$$V = \sum_0^{\infty} \beta_k \sum_{q=-k}^k A_k^q \langle r^k \rangle O_k^q \quad (1)$$

Where  $A_k^q \langle r^k \rangle$  is a parameter,  $O_k^q$  is the operator equivalent, and  $\beta_k$  represents a number, which depends on the number of f-electrons, and  $k$  is the rank of the matrix operator. The even  $k$  values account for the crystal field splitting and odd values represent intensity of the induced electric dipole transitions and this does not affect magnetism. The correct set of these parameters depend on the symmetry around the metal centre.<sup>[24]</sup> These are therefore closely related to the point group symmetry of the molecule. The modern crystal field Hamiltonian is expressed with the non-vanishing  $B_k^q$  parameters:

$$\hat{H}_{CF} = \sum_0^k \sum_{q=-k}^k B_k^q O_k^q \quad (2)$$

$B_k^q$  and  $A_k^q$  terms are inter-related and the new  $B_k^q$  and  $O_k^q$  terms are known as extended Stevens operators.<sup>[16,25]</sup> The axial crystal field (CF) parameters are denoted by the values of  $B_2^0, B_4^0, B_6^0$ , and  $B_2^{\pm 1, \pm 2}, B_4^{\pm 1, \pm 2, \pm 3, \pm 4}$ . terms denote non-axial or equatorial CF parameters. If the axial terms are higher in magnitude than the non-axial term it results in high magnetic anisotropy and shows large  $U_{\text{eff}}$ , while reverse case results in a ground state QTM.

## 2.2. Desired characteristics of the Crystal Field environment for Dy<sup>III</sup> SIMs

Earlier, we noted why Dy<sup>III</sup> ion is the most prominent candidate for producing SIMs and what type of crystal field is needed for this ion to obtain SIMs. Now we would like to highlight two of the most important factors regarding the crystal field environment that determines the SIM properties to a large extent. Simple model structures were studied by our group and Chibotaru et al. to find out what will lead to significant energy splitting between the ground to first and the other excited levels of the low lying  $m_J$  levels. The first approach is the strong axiality of the ligand environment, and the second is the role of symmetry around the metal ion to quench the QTM. The Dy<sup>III</sup> ion requires a strong axial field.<sup>[20,26]</sup> The modelled complex of  $[\text{DyO}]^+$  for which nuclear rotations and vibrations are the major or can say only cause for spin-phonon transition, can show the maximum calculated barrier around 2100  $\text{cm}^{-1}$ . Figure 2 represents the blocking barrier for this model where all the eight crystal field multiplets are involved and giving a theoretical barrier height that is equal to the total CF splitting of the atomic  $^6\text{H}_{15/2}$  multiplet. The highest possible performance of lanthanide-based SMMs thus can be achieved in the limit of a perfectly axial CF in these complexes.<sup>[27]</sup>

The above axiality of crystal field approach helps in justifying the SIM characteristics; however, it lacks in explaining QTM/TA-QTM effects which are the main contributor for relaxation phenomena for Dy<sup>III</sup> SIMs in the absence of other relaxation processes. The second important factor is the symmetry (or pseudo-symmetry) of coordination complex that is found to play a significant role in suppressing the QTM as highly symmetric molecules are found to be superior SIMs compared to less/unsymmetric one. Our group has earlier modelled a series of complexes for the Dy<sup>III</sup> as  $[\text{Dy}(\text{OH})_n]^{m\pm}$ , where the bond distance between Dy and O is at 2.3 Å, and the O–H bond length is fixed at 1 Å preserving the maximum symmetry permissible for all of the models to elucidate the role of symmetry and coordination environment in the magnetization relaxation processes. For lower coordination numbers such as 1 and 2, the Dy<sup>III</sup> complex shows very high axial anisotropy and  $m_J = \pm 15/2$  as the ground level, as equatorial ligation is absent. Hence the linear or pseudo-linear geometries (preserving  $C_{\infty v}$  and  $D_{\infty h}$  pseudo) symmetry are the best suited for the Dy<sup>III</sup> ion. The three ( $D_{3h}$ ) and four ( $D_{4h}$ ) coordinate Dy<sup>III</sup> models found to deteriorate the SIM characteristics as in these models, the additional ligand tends to occupy equatorial position(s) leading to reduction of CF splitting and enhancement of the transverse anisotropy—both contribute to faster relaxation. However, if higher symmetry is maintained, the  $g_z$  axes are collinear for all the 8 KDs offering a maximum observable barrier height of 800  $\text{cm}^{-1}$  for this model. This is still significantly less compared to linear geometries mentioned above. As long the axial ligands are stronger, the point groups such as  $C_{Nv}, D_{Nh}, S_8 (I_4), D_{4d}, D_{5h}$  and  $D_{6d}$  are superior even if ligands are present in the equatorial plane, as QTM found to be suppressed or quenched under this condition. This suggests the use of mixed donor type ligand with Oxygen and Nitrogen or Oxygen with differ-

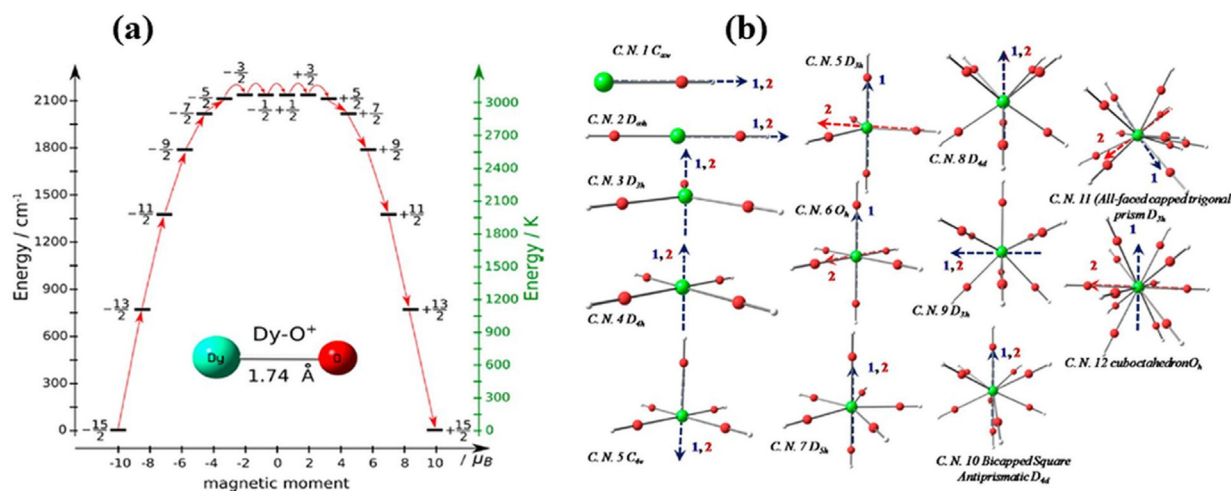


**Figure 2.** (a) The low-lying spectrum of all eight Kramers doublet of the  $[\text{DyO}]^+$ . The  $m_j$  values for corresponding multiplets are written with numbers beside the bold horizontal line. The arrows represent the allowed spin-phonon transitions. (b) All Modelled structures for  $\text{Dy}^{\text{III}}$  with CN 1 to 12. Adapted with the permission from Ref. [24] and Ref. [33].

ent donor strength. This idea has been employed to obtain high-blocking SIMs with  $D_{5h}$  and  $D_{6d}$  symmetry possessing pentagonal bipyramidal and quasi octahedral geometries, respectively.<sup>[26,28]</sup> Ab initio calculations reveal that the quasi- $D_{5h}$   $\text{Dy}^{\text{III}}$  ion with strong axial ligand and weak or moderate equatorial ligation possesses Ising ground state with large barrier height for magnetisation reversal compared to the less axial quasi- $O_h$ -symmetry geometry.<sup>[14a]</sup>

The discovery of Ln-SMM with carbon donor centre in 2010, makes to rethink about the engagement organometallic complexes with SMM.<sup>[10c]</sup> Two most important class of ligands in this regard are the cyclopentadienyl( $[\text{Cp}]^-$ ) and cyclooctatriene ( $[\text{COT}]^{2-}$ ) dianion using which many lanthanide-based SIMs/SMMs are reported. Further, other ligands such as cyclo-arenes

as well as fullerene also been utilised in recent years to develop new generation SIMs. Before we begin, we would like to put forth the nature of Ln-C interaction and how they could potentially yield very large blocking barriers. To assess this we have constructed the mechanism of magnetic relaxation for two toy models  $[\text{Dy}(\text{CH}_2)_2]^{3+}$  (model a) and  $[\text{Dy}(\text{CH}_3)_2]^+$  (model b) using the established methodology<sup>[29]</sup> and these are shown in Figure 3 (see ref. note).<sup>[30]</sup> With both ligands, the linear geometry is maintained and yield huge blocking barrier with QTM being quenched up to the 4th excited state (at this level the computed tunnelling probabilities are much higher compared to other lower levels, example 2.6 vs. 0.06 for model a, see Figure 3). This is also supported by the coefficient calculated using Direct process (black number connecting various  $m_j$

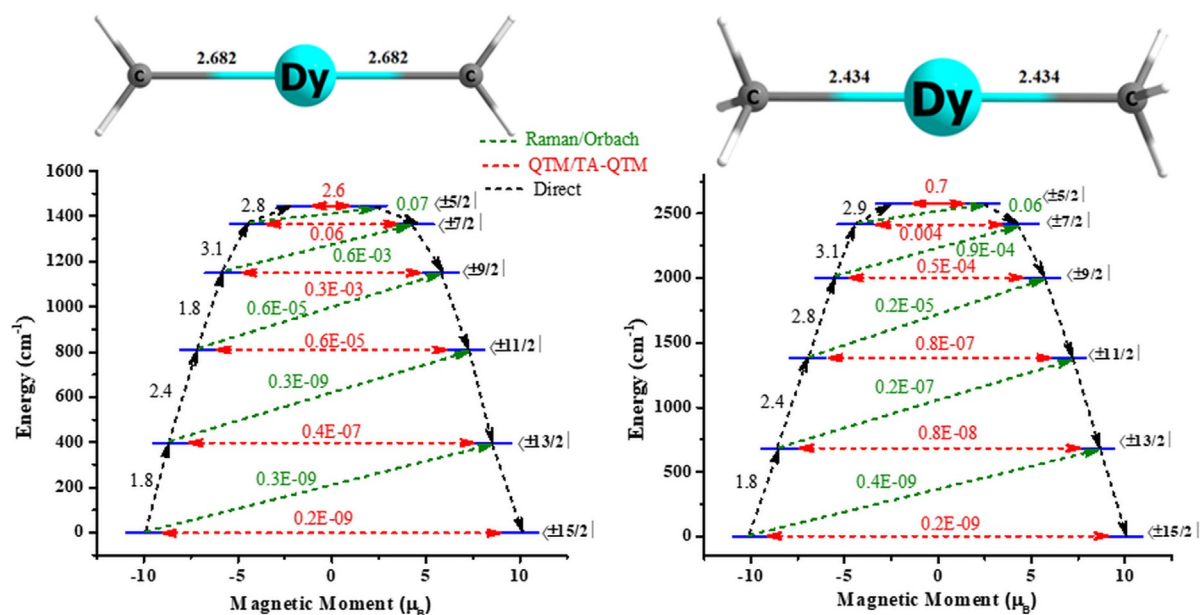


**Figure 3.** Ab initio computed energy of Kramers doublets, various transition possibilities along with the relaxation mechanism on the models a and model b. See texts and Table 1 for further details.

levels with larger number suggesting greater probability). The ground state  $g$ -anisotropies are ideal Ising values with  $g_x, g_y = 0.000$  and  $g_z = 20.000$  for both models with a pure  $m_j = \pm 15/2$  ground state (see Table 1). The overall crystal field splitting, however, is different for the two models with carbene-type ligand yield a barrier height of  $1447 \text{ cm}^{-1}$  while anionic  $\text{CH}_3^-$  yield  $2577 \text{ cm}^{-1}$ . This reveals the importance of the anionic carbon-based ligand in enhancing the crystal field strength and hence the overall barrier height for the reorientation of magnetisation. Anionic ligand not only provides greater crystal field splitting but also offer shorter Dy-C distances compared to neutral carbene-based ligand framework.

**Table 1.** Ab initio calculated  $g$ -tensors, energies, and the angle between the  $g_z$  axes for models a and b.

Complex	$g_x$	$g_y$	$g_z$	Energy [ $\text{cm}^{-1}$ ]	Tilt angle with respect to $g_z$ [ $^\circ$ ]	$U_{\text{cal}}$ [ $\text{cm}^{-1}$ ]
Model a GS	0.000	0.000	20.000	0.00		
Model a 1st ES	0.000	0.000	17.128	395.3	0.0	
Model a 2nd ES	0.000	0.000	14.264	807.2	0.0	
Model a 3rd ES	0.001	0.001	11.565	1150.0	0.0	
Model a 4th ES	0.168	0.197	8.908	1364.9	0.0	
Model a 5th ES	3.914	5.635	10.209	1447.6	90.0	1447.6
Model b GS	0.000	0.000	20.000	0.0	0.0	
Model b 1st ES	0.000	0.000	16.931	677.9	0.0	
Model b 2nd ES	0.000	0.000	13.909	1380.9	0.0	
Model b 3rd ES	0.000	0.000	11.179	2005.9	0.0	
Model b 4th ES	0.012	0.012	8.833	2418.7	0.0	
Model b 5th ES	1.844	2.224	4.968	2577.0	20.0	2577

### 2.3. Cyclo-arene based $\text{Ln}^{\text{III}}$ SIMs

Organo-lanthanide complexes have gained attention in recent years and are relatively scarce compared to conventional lanthanide coordination complexes. Here we have attempted to highlight the examples where theoretical tools have been used extensively to gain an in-depth understanding of the mecha-

nism of relaxation and at the same time also the nature of Ln–C bonding. To understand the nature of anisotropy in pure organometallic Ln SMM, it is important to see the effect of C donation to the Ln centres. This was done comprehensively by our group through ab initio CASSCF/RASSI-SO/SINGLE ANISO studies on series of trigonal prismatic  $[\text{M}(\text{BcMe})_3]$  ( $\text{M} = \text{Tb}(\mathbf{1a}), \text{Dy}(\mathbf{1b}), \text{Ho}(\mathbf{1c}), \text{Er}(\mathbf{1d})$ ),  $[\text{BcMe}]^- = \text{dihydrobis(methylimidazolyl)borate}$  complexes (see Figure 4).<sup>[29a]</sup> Among these, the Tb and Dy analogues yield theoretical barrier height of  $256.4$  and  $268.5 \text{ cm}^{-1}$  respectively. This lesson transpire improved SIM behaviour of carbene analogue because of axially compressed trigonal prismatic ligand environment.<sup>[31]</sup> The  $g$ -tensor computed for the ground and first excited state along with the theoretical estimate of the barrier heights and the  $U_{\text{eff}}$  values estimated using experiments for the above four complexes are provided below in Table 2. In the same study for comparison, calculations have been performed on pyrazole based nitrogen donor ligand and in this case, both the overall crystal field as well as the estimated barrier heights are smaller compared to the imidazole C-donor ligands suggesting how important to keep Ln–C interaction to enhance the barrier height. To probe the nature of Ln–C bonding, DFT calculations have been performed and this reveals that the six coordinated C atom possesses a small negative spin density which suggests a dominant spin-polarization mechanism. The strong crystal field around the carbene ligand was predicted from the Mulliken charge analysis. More importantly the agostic B–H...Ln<sup>III</sup> interactions present in these complexes found to play a critical role in controlling the anisotropy beyond the Ln–C bonding.

Another very important organometallic-Dy<sup>III</sup> complex synthesized and theoretically studied by Y.-N. Guo, et al. on  $[\text{Dy}(\text{NCN})\text{Cl}_2(\text{THF})_2]$  complex (complex  $\mathbf{2}$ ),<sup>[32]</sup> where NCN represents a pincer ligand. This complex showed a barrier height of  $262 \text{ cm}^{-1}$  computed from CASSCF-RASSI-SO-SINGLE ANISO and the magnetization relaxation occurs from the second ex-

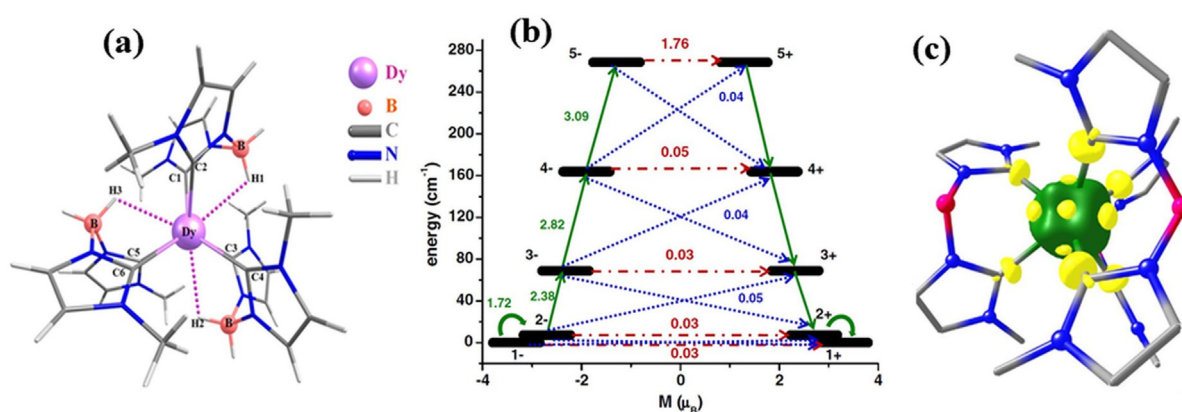


**Figure 4.** (a) The crystal structure of the complex  $\mathbf{1b}$ . (b) Ab initio computed magnetic blocking barrier as a function of magnetic moment for the same (The blue dotted lines indicate the Orbach process, the solid green arrows imply Raman/Orbach, the dashed-dotted red lines correspond to QTM/TA-QTM and the numbers at each arrow are the mean absolute value for the corresponding transition matrix element of magnetic moment). (c) Green and yellow regions correspond to positive and negative spin densities, respectively. Adapted with the permission from Ref. [29a].

**Table 2.** The calculated ground and  $n^{\text{th}}$  excited state energy values up to where magnetisation is relaxed, corresponding  $g$ -tensors and angles ( $\theta$ ) of the principal anisotropy axis of the  $n^{\text{th}}$  excited state with respect to the ground state (for complexes **1b** and **1d** these are Kramers doublet (KD), and for **1a** and **1c** these are pseudo doublet).

Complexes	g-factors			Energy [ $\text{cm}^{-1}$ ]	Tilt angle with respect to $g_z$ $\theta$ [ $^\circ$ ]	$U_{\text{cal}}$ [ $\text{cm}^{-1}$ ]	$U_{\text{eff}}$ [ $\text{cm}^{-1}$ ]	Ref.
<b>1a GS</b>	$g_x$	$g_y$	$g_z$	0.000 0.000 17.930 0.0 and 0.02				
	0.000	0.000	14.650	256.36	256.39	0.01	256.36	44.8
<b>1b GS</b>	0.070	0.090	19.910	0.0				
<b>1b 1st ES</b>	0.010	0.180	17.310	7.27		2.73	268.50	32.8
<b>1c GS</b>	9.640	9.330	1.080	0.0 and 0.04				[29a]
<b>1c 1st ES</b>	0.080	0.240	3.170	9.01 and 12.05	0.01	9.01	-	
<b>1d GS</b>	0.580	1.730	3.660	0.0				
<b>1d 1st ES</b>	0.510	0.700	3.770	23.29	0.71	23.29	-	
<b>2 GS</b>	0.001	0.002	19.810	0.0				
<b>2 1st ES</b>	0.001	0.003	17.069	176	0.0			[32]
<b>2 2nd ES</b>	0.426	0.437	19.444	262	90.0	262	233	
<b>3 GS</b>	0.00	0.00	19.88	0				
<b>3 1st ES</b>	0.00	0.00	17.19	168	3.89			
<b>3 2nd ES</b>	0.09	0.14	14.27	399	1.56			[33]
<b>3 3rd ES</b>	2.09	5.61	14.11	516	85.37	516	501	
<b>3 4th ES</b>	1.32	4.36	12.34	563	83.41	563	565	
<b>4a GS</b>	0.007	0.011	17.820	99.8*	1.49	-	95.6	
<b>4b GS</b>	0.009	0.015	17.747	90.1*	2.61	-	102.9	
<b>4c GS</b>	0.002	0.005	17.707	89.8*	6.25	-	107.1	[34]
<b>4d GS</b>	0.000	0.001	17.722	138.0*	0.74	-	133.6	
<b>5a GS</b>	0.000	0.000	17.959					
<b>5a 1st ES</b>	0.000	0.000	15.530	175-187	1.0			
<b>5a 2nd ES</b>	9.986	9.153	1.222	194-202	-		199	[35]
<b>5b GS</b>	0.062	0.145	12.644					
<b>5b 1st ES</b>	0.000	0.058	13.843	21-23	21.4		7.6	
<b>6a GS</b>	0.000	0.000	17.944	0.0				
<b>6a 1st ES</b>	0.002	0.003	15.527	184.0	0.49			
<b>6a 2nd ES</b>	10.092	9.011	1.220	280.4	0.33	280.4		
<b>6b GS</b>	0.000	0.000	17.941	0.00				
<b>6b 1st ES</b>	0.001	0.001	15.509	164.5	0.0			[36]
<b>6b 2nd ES</b>	9.900	9.187	1.248	247.07	1.24	247.1		
<b>6c GS</b>	0.000	0.000	17.920	0.00				
<b>6c 1st ES</b>	0.510	0.880	15.610	169.22	49.48	169.2		
<b>6d GS</b>	2.433	2.433	1.033	0.0	-			[21]
<b>7a GS</b>	0.000	0.000	19.890					
<b>7a 1st ES</b>	0.000	0.000	17.020	488.6	1.9			
<b>7a 2nd ES</b>	0.000	0.000	14.400	771.0	2.9			
<b>7a 3rd ES</b>	0.000	0.010	11.760	956.5	3.3			[11c]
<b>7a 4th ES</b>	0.050	0.050	9.110	1122.2	4.9			
<b>7a 5th ES</b>	0.830	1.010	6.440	1277.5	3.4	1277.5	1223	
<b>7b GS</b>	0.000	0.000	20.004					
<b>7b 1st ES</b>	0.000	0.000	16.939	672	2.3			
<b>7b 2nd ES</b>	0.007	0.007	14.354	1061	4.2			[11a]
<b>7b 3rd ES</b>	0.034	0.046	11.746	1304	2.6			
<b>7b 4th ES</b>	0.053	0.136	9.060	1524	5.3	1524	1541	
<b>8 GS</b>	0.008	0.013	19.734	0.0				
<b>8 1st ES</b>	0.847	2.069	14.995	284	7.1	284	323	[38]
<b>9b GS</b>	0.001	0.002	19.979	0.0				
<b>9b 1st ES</b>	0.083	0.120	17.119	244.5	7.7			[42]
<b>9b 2nd ES</b>	0.603	0.663	14.152	357.2	173.1	357.2		

\*Energy difference between ground state (GS) KD and 1st excited state (ES) KD.

cited state via Orbach followed by thermally assisted QTM process (see Table 2 and Figure 5). The experimental fitting of ac data with Arrhenius fit revealed an effective energy barrier height of  $233 \text{ cm}^{-1}$  ( $U_{\text{eff}}$ ) which agrees nicely with CASSCF com-

puted values ( $U_{\text{cal}}$ ). The computed  $g_z$  angle at the respective Kramers doublets (KDs) shows that the  $g_z$  axis remains parallel to the ground state  $g_z$  axis up to first excited but becomes perpendicular at the second excited state. The molecule has  $C_{2v}$  core symmetry and the proper  $C_2$  axis passes along the Dy–C bond axis. A stronger crystal field of the carbene (NCN) compared to the weaker halide is the driving factor to show such high  $U_{\text{eff}}$ . This proposed relaxation mechanism for the first time offered a new pathway to enhance the  $U_{\text{eff}}$  in a molecule possessing sufficient axial symmetry.

By increasing the bond order from Dy–C single bond to very strong Dy=C double bond (methanediide coordination) at the axial position which is observed in  $[\text{Dy}(\text{BIPM}^{\text{TM}})_2][\text{K}(\text{18C6})(\text{THF})_2]$  (complex **3**) reported by Liddle and co-workers in 2016 (see Figure 6).<sup>[33]</sup> This molecule shows a zero-field frequency and temperature-dependent SIM behaviour with two thermally activated  $U_{\text{eff}}$  value of 721 K ( $501 \text{ cm}^{-1}$ ) and 813 K ( $565 \text{ cm}^{-1}$ ). The CASSCF-RASSI-SO-SINGLE ANISO calculation suggests a relaxation through thermally activated third excited state KD and fourth excited KD with an energy barrier of  $516 \text{ cm}^{-1}$  and  $563 \text{ cm}^{-1}$  respectively (see Table 2). The strong C=Dy=C bond at the axial position keeps the magnetic axis ( $g_z$  axis) align parallel up to second excited KD. The computed anisotropy barrier matches quite well with the experimental ac fit data. Furthermore, luminescence (optical emission spectroscopy) studies have also been carried out to investigate the energy gap between different J states. The ab initio calculations here also nicely reproduce the  $J=15/2 \leftrightarrow 13/2$  gap obtained from the emission spectra.

Moving from carbene to arene, among all the organolanthanide SMM, the complexes with the  $\text{COT}^{2-}$  and  $\text{Cp}^-$  were very much dominating.<sup>[10b,17,19]</sup> The computational studies on these systems reveal the magnetic relaxation, anisotropy, the role of higher-order symmetry, electrostatic crystal field design, the strategy of coupling the rings to observe the relaxation dynamics, the exchange between the metal ions coupled via a ring etc. in much more details. The  $\pi$  cloud of the cycloarene ligand can donate its delocalised electrons to the  $\text{Ln}^{\text{III}}$  thus by making strong axial crystal field and mimicking a pseudo-linear geometry. To begin with, we expand the coordination sphere to include the arene along with other conventional ligands to explore the half sandwich organometallic complexes. The starting series of a complex in this regard is the  $[\text{Er-COT}]^-$  half-sandwich complexes, where one side is coordinated to the  $\text{COT}^{2-}$  and the other side to a halide or oxo-donor ligands. Four complexes of this kind has been reported as  $[\text{Er}(\text{COT})\text{I}(\text{THF})_2]$ , (THF = tetrahydrofuran) (**4a**),  $[\text{Er}(\text{COT})\text{I}(\text{Py})_2]$  (Py = pyridine) (**4b**),  $[\text{Er}(\text{COT})\text{I}(\text{MeCN})_2]$  (MeCN = acetonitrile) (**4c**), and  $[\text{Er}(\text{COT})(\text{Tp}^*)]$  ( $\text{Tp}^* = \text{tris}(3,5\text{-dimethyl-1-pyrazolyl}) \text{ borate}$ ) (**4d**)



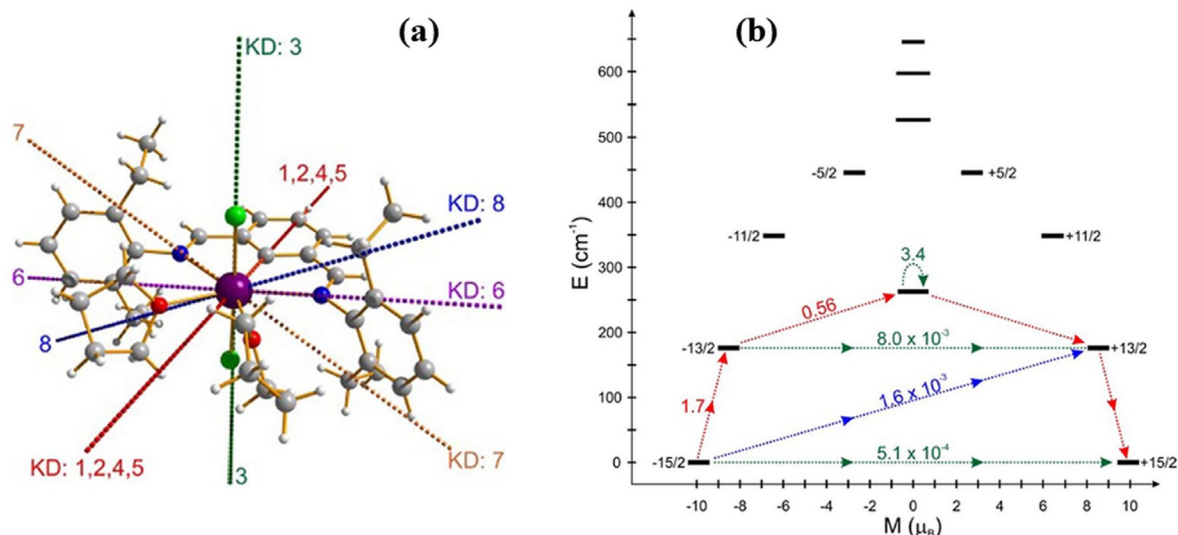


**Figure 5.** a) Ab initio computed  $g_z$  orientations for different Kramer's doublet for complex 2 (KD: 1–8 ranked in order of the energy from ground state to the seventh excited state- the red dashed line corresponds to the anisotropy axis of KD: 1, 2, 4 and 5; the green dashed line shows the anisotropy axis of the second excited KD) and b) ab initio computed energies of the KDs showing the relaxation mechanism of complex Anisotropy axes in eight lowest Kramer's doublets at the Dy site of DyNCN (KD 3 lying at  $262\text{ cm}^{-1}$ ). The arrows represent the averaged matrix element of the transversal magnetic moment connecting the corresponding states. Figures reproduced with the permission taken from Ref. [32].

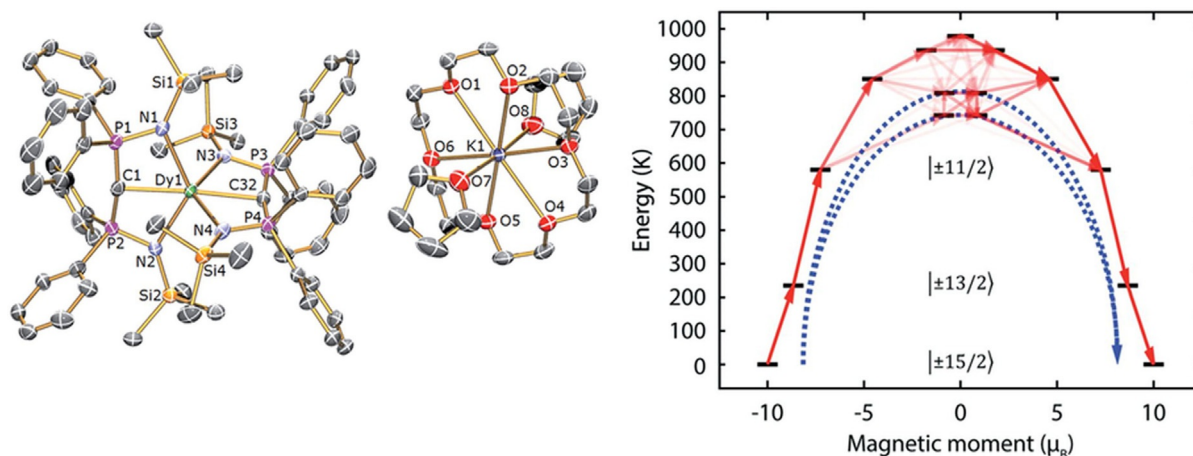


**Figure 6.** Crystal structure of complex 3 (left) and corresponding CASSCF-RASSI-SO computed barrier height of the same (right). The red arrows indicate the transition probabilities within the respective KDs and blue dotted arrows show the relaxation pathway through third and fourth excited KDs. Adapted with the permission from Ref. [33].

where the COT ligand has been kept intact and other conventional ligands are systematically varied. All these four complexes are found to show SIM behaviour with  $U_{\text{eff}}$  of 95.6(9), 102.9(3.1), 107.1(1.3), and  $133.6(2.2)\text{ cm}^{-1}$  for **4a–4d**, respectively.<sup>[34]</sup> Mechanism of magnetisation relaxation developed for these complexes is shown in Figure 7. The crystal field exerted by the  $\text{COT}^{2-}$  ligand found to be dominating in all four complexes with the  $\text{COT}^{2-}$  dictating the direction of the  $g_z$  axis (see Table 2 for the computed parameters for **4a–4d**) and stabilising  $m_J = \pm 15/2$  as the ground state in all cases. While complexes **4a–4c** found to possess very similar magnetic characteristics ( $g$  tensors, ground-state-first excited state gap), complex **4d** found to have smallest transverse  $g$ -component

and larger ground state first excited state gap computed from CASSCF-RASSI-SO. This suggests that Iodine ligand being present in all the other three cases likely to play as a spoiler.

As the  $\text{Cp}^-$  and  $\text{COT}^{2-}$  are the two most potential ligands for generating organolanthanide type SIM, both  $\text{Dy}^{\text{III}}$  and  $\text{Er}^{\text{III}}$  sandwiched between these two corresponding ligand framework and their magnetic properties were studied explicitly by several groups.<sup>[17]</sup> Depending on the size of the ring, the approach of ligand to the  $\text{Ln}^{\text{III}}$  metal ion varies substantially. This has been summarised below by comparing different molecules and models. One of the best SIM with  $\text{Er}^{\text{III}}$  till date known has been reported with the  $\text{COT}^{2-}$  ligand with an  $U_{\text{eff}}$  of  $\approx 199\text{ cm}^{-1}$  as it is facing the ligand in an equatorial fashion

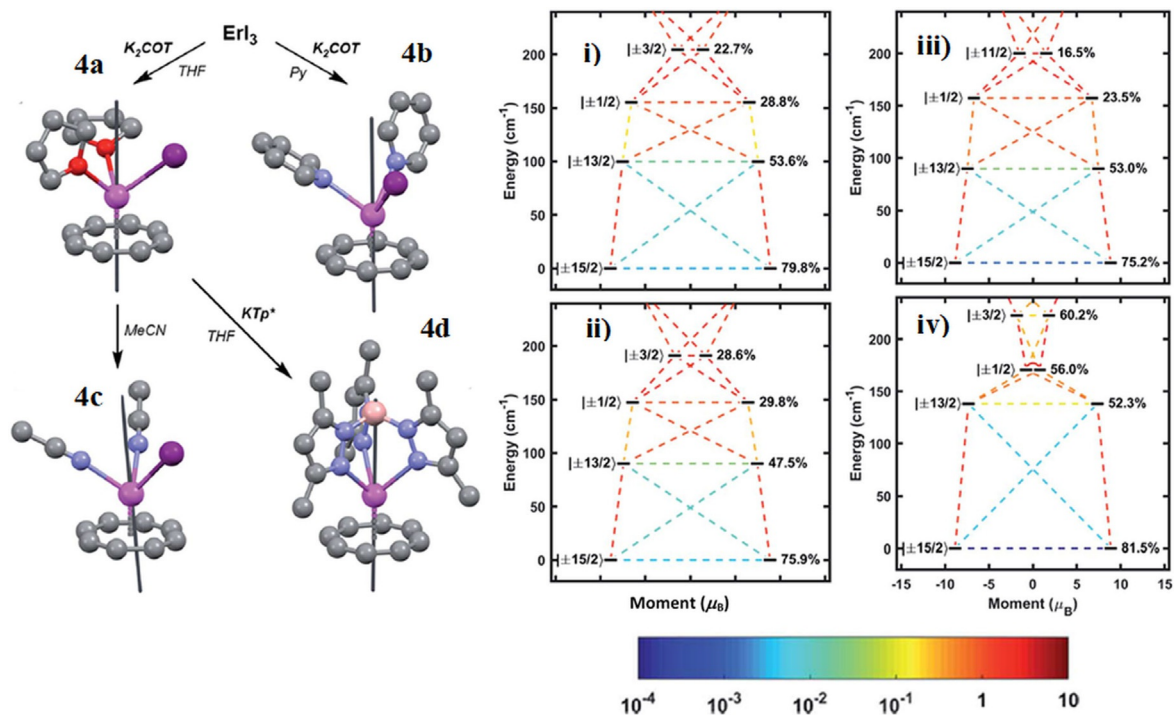


**Figure 7.** The core of half-sandwich complexes **4a–4d** and schematic representation of their synthesis (left). The energy spectra calculated by ab initio method for the four lowest Kramer doublets plotted against function of their magnetic moments for (i) **4a**, (ii) **4b**, (iii) **4c** and (iv) **4d**. The states are labelled by their largest contributing  $m_j$  component (left) and the percentage of that component (right). Adapted with the permission from Ref. [34].

confirming from the crystal field parameter (see Figure 8). For this  $[\text{Er}(\text{COT})_2]^{2-}$  (**5a**) complex the ground state is found to be  $m_j = \pm 15/2$  in nature. It is noted that the Ising nature of the ground state anisotropy, however, vanishes for the  $\text{Er}^{\text{III}}$  moving from eighth to five-membered ring whereas the reverse occurs for  $\text{Dy}^{\text{III}}$ . The energy splitting for  $[\text{Dy}(\text{COT})_2]^-$  (**5b**) from the CASSCF-RASSI-SO shows that the ground state is no more of  $\pm 15/2$  type rather it is  $\pm 9/2$  having significant Raman/Orbach transition probability at the first excited level showing an energy barrier of  $\approx 9 \text{ cm}^{-1}$  only. For the oblate  $\text{Dy}^{\text{III}}$  ion, increasing the ring size to  $\text{COT}^{2-}$  lead to strong equatorial donations, and this causes the crystal field splitting to be reduced significantly also generating transverse anisotropy for the low lying KDs resulting in a drastic decrease of  $U_{\text{eff}}$  value. Additionally, due to the nature of the interaction, the excited state has strong tunnelling leading to very small barrier height for magnetisation reversal (see Table 2 for computed parameters).  $\text{Er}^{\text{III}}$  being a prolate species rather enjoys this equatorial donation and therefore shows large  $U_{\text{eff}}^{\text{[35]}}$ .

The  $\text{Er}^{\text{III}}$  based SIM within the above-mentioned kind of environment was studied further in detail by our group by varying the nature of the ligands attached to the  $\text{Er}^{\text{III}}$  centre. Here three  $\text{Er}^{\text{III}}$  SIMs are studied namely  $[\text{Er}(\text{COT})_2]^-$  (**6a**) and  $[\text{Er}(\text{COT}^*)_2]^-$  (**6b**) (here  $\text{COT}^* = 1, 4\text{SiMe}_3$  substituent in COT) and  $[\text{ErCp}^*(\text{COT})]$  (**6c**) (see Figure 9).<sup>[36]</sup> The SINGLE-ANISO studied after the CASSCF-RASSI calculations show that replacing  $\text{Cp}^*$  with  $\text{COT}^{2-}$  cause a decrease in the  $U_{\text{cal}}$  value whereas introducing some bulky group like trimethylsilyl at a certain position can also decrease the  $U_{\text{cal}}$ , though the decrease is not that

significant as that in the case for complex **6c**. In all the three cases, the ground state  $g$ -tensor is pure Ising type with computed  $g_z$  values  $\approx 18$  and it becomes non-Ising, moving to higher-level KDs that is, second excited state(s) (see Table 2). The CASSCF-RASSI-SO computed barrier height are  $280 \text{ cm}^{-1}$ ,  $247 \text{ cm}^{-1}$  and  $169 \text{ cm}^{-1}$  for complexes **6a**, **6b** and **6c**, respectively. The  $g_z$  axis which is found to be passing through the principal  $C_8$  axis despite significant negative charge on the carbon atoms (obtained from DFT). Though the  $C_2$  axes perpendicular to  $C_8$  axis is less repulsive in terms of electrostatic interaction, the  $g_z$  still pass through the  $C_8$  (or pseudo  $C_8$  in case of **6b**) as the overall symmetry and the unique directionality of the  $g_z$  needs to be maintained. This is in accord with the fact that anisotropy is found to be aligned along the principal axis of symmetry, independent of the electrostatic repulsion.

Although DFT calculations cannot account for the anisotropy that is arising due to multi-configurational character of the wavefunction, it is useful to analyse the lanthanide-ligand bonding as this feature is absent in restricted active space calculations. Qualitative molecular orbital (MO) diagram developed for complex **6a** is shown in Figure 10. Of particular relevance, here is the splitting of  $\beta$  MOs as this is strongly correlated to the nature of the  $m_j$  ground state observed. Particularly the COT  $\sigma^*$  orbitals are found to interact with the  $4f \beta$  MOs leading to larger splitting and this was qualitatively correlated to the observed anisotropy obtained from the ab initio calculations. Computed spin density plot (Figure 10b) reveals that dominant spin delocalisation of spins on the  $\pi^*$  orbitals of COT

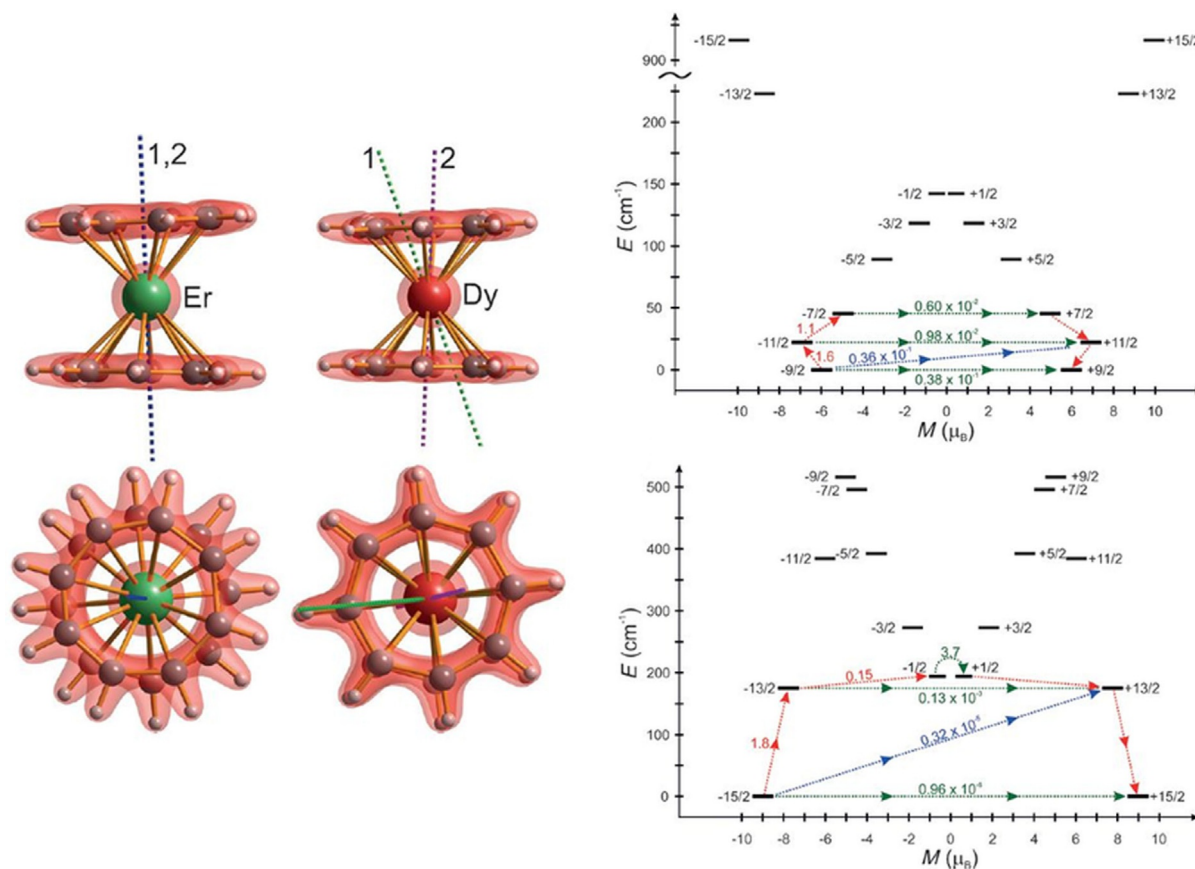


**Figure 8.** Structure of complex **5a** (top left of side view, bottom left top view) and **5b** (top right side view, bottom right view) This shows ab initio constructed magnetization blocking barriers for complex **5b** (top right Dy) and **5a** (bottom right Er). Adapted with the permission from Ref. [35].

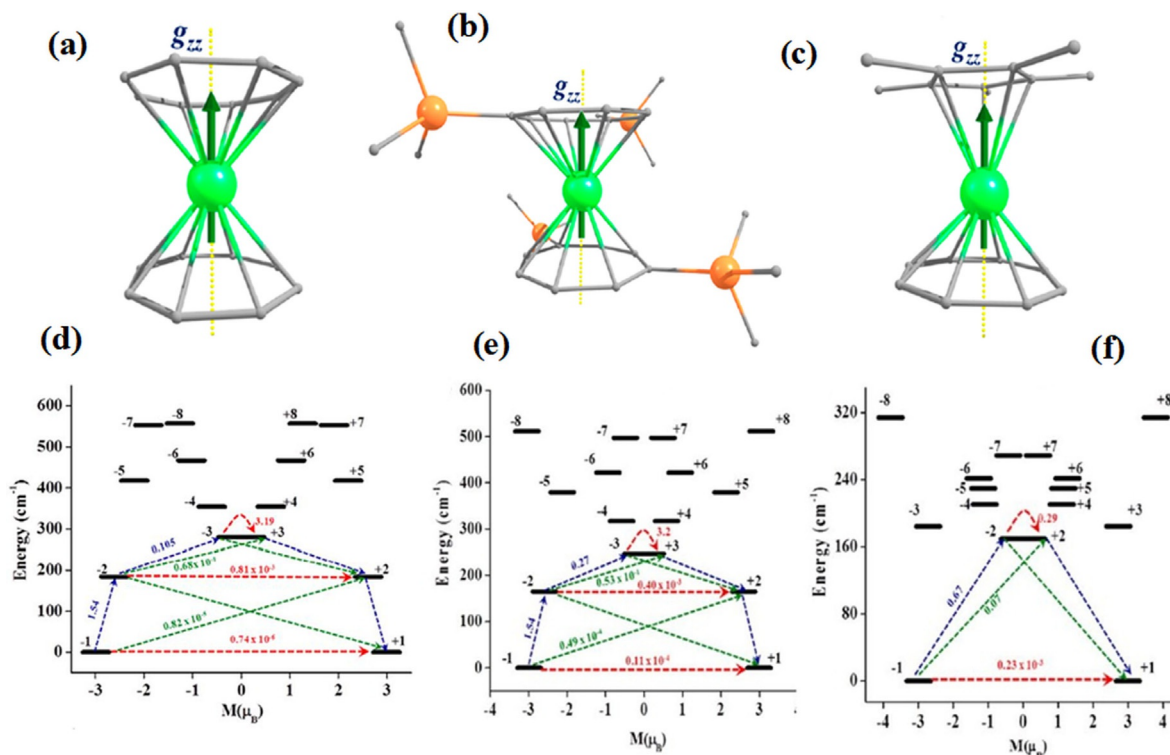


**Figure 9.** Structure of complex **6a**, **6b** and **6c**. Green = Er, Grey = C, Orange = Si with arrangement of main magnetic axis and ground state anisotropic axis. Corresponding ab initio computed magnetization relaxation mechanism (d) **6a**, (e) **6b** and (f) **6c**. Adapted with the permission from Ref. [36].

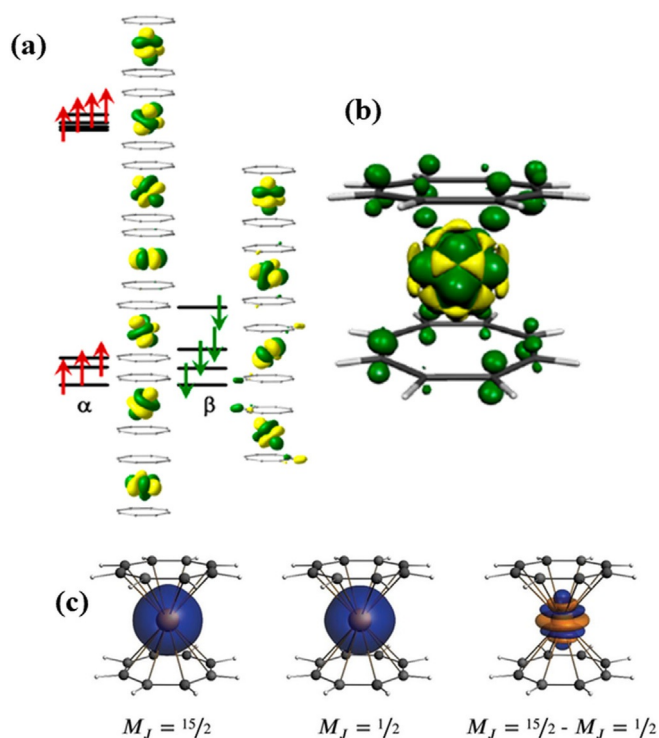


**Figure 10.** (a) The  $\alpha$  and  $\beta$  MOs of the 4f-orbitals with their corresponding Eigenvalues for complexes Er-COT and (b) The spin density plot computed using DFT. The isosurface represented corresponds to a value of  $0.005 e^- \text{ bohr}^{-3}$ . The green and yellow regions indicate positive and negative spin densities, respectively. (c) Electron density of  $m_j$  levels of  $[\text{Er}(\text{COT})_2]^-$  computed using ab initio calculations employing isosurface at  $\pm 0.001$  au. Adapted with the permission from Ref. [36] and Ref. [37].

ligand and this is different to that observed for other types of ligands. Besides the axial  $B_{2,4,6,0}$  terms of the crystal field parameters found to decrease in the same order ( $6\mathbf{a} > 6\mathbf{b} > 6\mathbf{c}$ ) as

that of the computed  $U_{\text{cal}}$  value.<sup>[36]</sup> Recently electron density of the 4f configuration with their spin and orbital magnetization were obtained using ab initio calculations taking into account the SOC. These densities were plotted for various  $[\text{Ln}(\text{COT})_2]^-$  systems offering insight into the nature of  $m_j$  (in Figure termed as  $M_j$ ) level densities and their projection (see Figure 10c) offering clue in the way one can design SIMs.<sup>[37]</sup>

Apart from the  $\text{Dy}^{\text{III}}$  and  $\text{Er}^{\text{III}}$  ion, another marking work with  $\text{Ce}^{\text{III}}$  has been computationally explored for  $[\text{Li}(\text{DME})_3][\text{Ce}^{\text{III}}(\text{COT}'')_2]$  (**6d**) (DME = dimethoxyethane,  $\text{COT}'' = 1,4$ -bis(trimethylsilyl)cyclooctatetraenyldianion) which has  $U_{\text{eff}}$  value of  $21 \text{ cm}^{-1}$  at an applied magnetic field (see Figure 11).<sup>[21]</sup> The ground state  $m_j$  here corresponds to  $\pm 1/2$  state. This clearly suggests that the COT crystal field with a strong equatorial donation is unsuitable for  $\text{Ce}^{\text{III}}$  ion, which is suggested to be oblate type by qualitative analysis.<sup>[37]</sup> The computed g tensors for the ground state KDs are  $g_x = 2.432$ ,  $g_y = 2.361$  and  $g_z = 1.033$ ; this reflects a pure rhombic set of g tensors with a small magnetic moment along the easy axis. The computed orientation of the  $g_z$  axis is collinear with the highest symmetric axis. However, the large rhombic anisotropy enhances the QTM between the ground levels states and the SMM behaviour is observed at applied field only.

As we have revealed above that the smaller member ring-like Cp and Cp\* are the best organometallic ligand for  $\text{Dy}^{\text{III}}$ , the last two year witnessed two of the most recognisable work till date with  $\text{Dy}^{\text{III}}$ Cp\* complexes **7a**  $[(\text{Cp}^{\text{III}})_2\text{Dy}]^+$  and **7b**  $[(\text{Cp}^{\text{Pr5}})\text{Dy}(\text{Cp}^*)]^+$  with the blocking temperature of 60 K and 80 K respectively with the record energy barrier of  $1277 \text{ cm}^{-1}$  and  $1541 \text{ cm}^{-1}$  (see Figure 12 and 13).<sup>[11a-c]</sup> The structures are provided below. Apart from these two molecules one more of this kind is reported by Long et al. having the molecular formula  $[\text{Dy}(\text{Cp}^{\text{Pr4Me}})_2][\text{B}(\text{C}_6\text{F}_5)_4]$  (**6c**) with an effective blocking barrier of  $1468 \text{ cm}^{-1}$  and blocking temperature of 72 K.<sup>[11d]</sup>

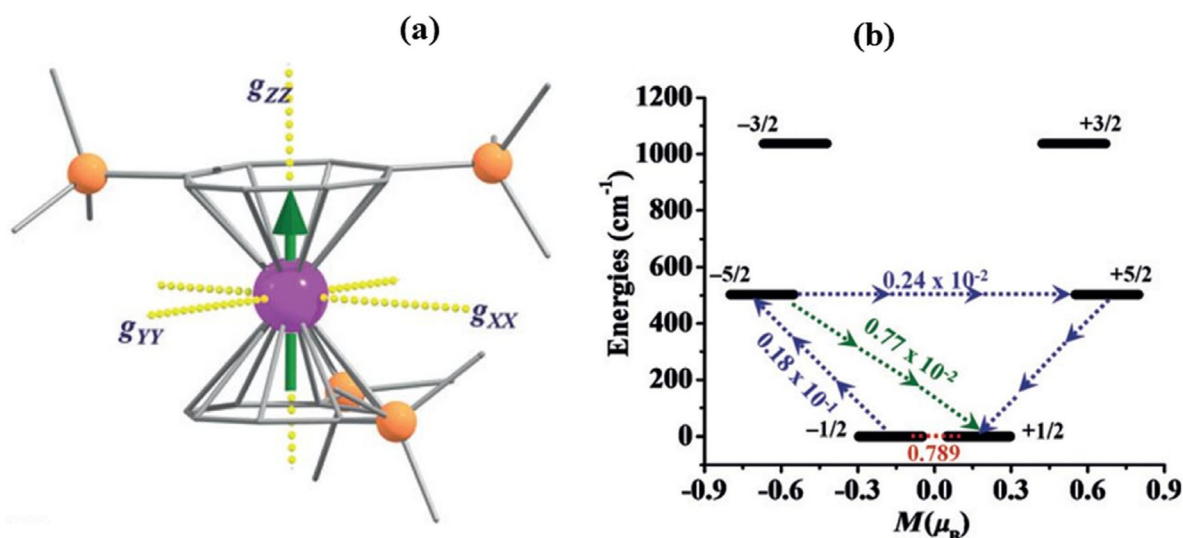


**Figure 11.** (a) X-ray structures of complex **6d** showing ab initio computed orientations of the g tensors of the ground-state KDs. Colour code: pink, Ce; grey wires, carbon; orange, Si. Hydrogen atoms are omitted for clarity. (b) Ab initio computed magnetisation blockade barriers (overestimates than the experimental  $U_{\text{eff}}$ ) along with calculated transversal magnetic moments between the connecting pairs for the complex. This is one of the unconventional field-induced SMM excluding the Dy and Er. Adapted with the permission from Ref. [21].

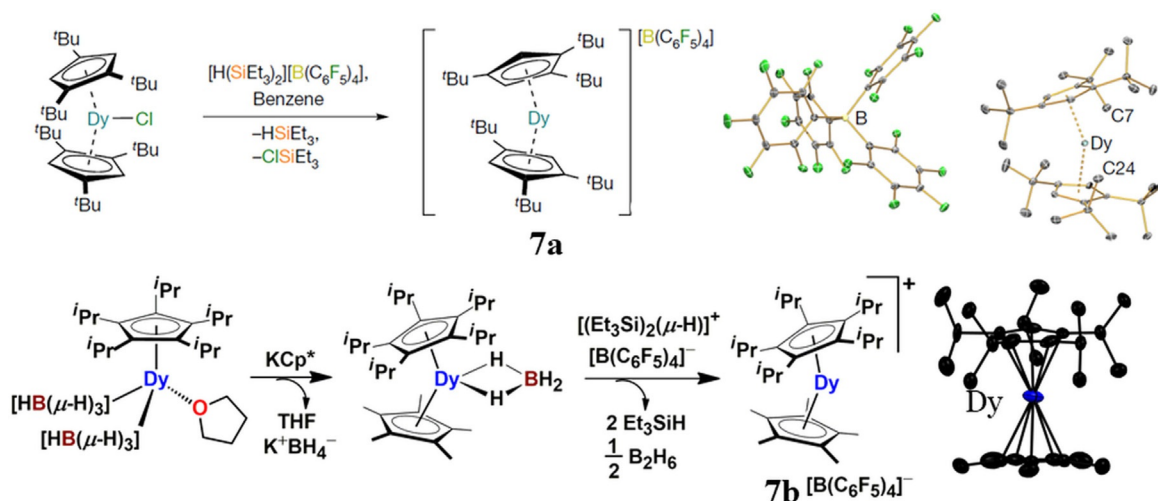


**Figure 12.** Synthesis Scheme and X-Ray structures of complex **7a** and **7b** (for clarity, the hydrogen atoms are omitted). Adapted with the permission from Ref. [11c].

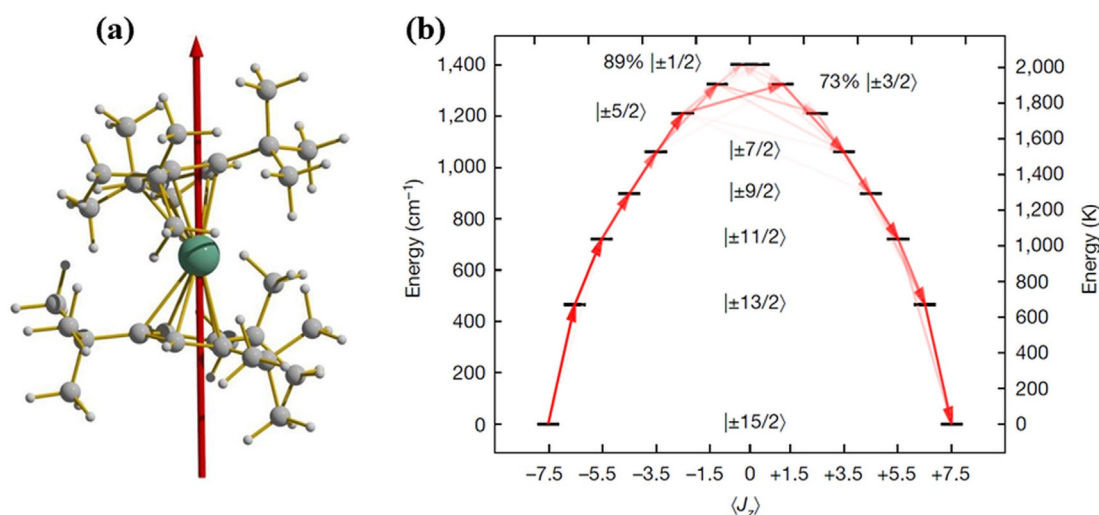


**Figure 13.** Arrangement of anisotropic axis for complex **7a** (a) and relaxation dynamics of complex **7a** (b). The energy is plotted as a function of KD and the mechanism of expected relaxation was shown. Adapted with the permission from Ref. [11b–c].

As the two molecules are believed to be setting the trend in this field, their theoretical investigation can give some fruitful result to understand the mechanism of relaxation. This has been achieved using wavefunction based multi-reference calculations in the above example. The computational aspect shows that the arrangement of anisotropic axes remained coincident with the ground state, up to 5th excited state for **7a** and 4th excited state for **7b** and thus maintaining a large Ising anisotropy at the higher level also and the transverse component barely contributes up to the 4th excited state (see Table 2). This is due to the pseudo-linear arrangement of the Cp' ligand and its derivatives mimicking a perfectly axial crystal field environment which is confirmed by analysing the crystal field parameter.

For both the molecules **7a** and **7b**, the behaviour is quite similar, though the latter shows better  $U_{\text{eff}}$  and  $T_B$  because of

the bulkier isopropyl group, which can cause a better donation of the electron to the aromatic ring which acts as an axial crystal field to the Dy<sup>III</sup> ion. The bulkiness further increases the angle between the ring to  $\approx 163^\circ$  than its congener  $\approx 153^\circ$  leading to increase in  $U_{\text{eff}}$ . Despite showing such high ground to first excited state energy difference still,  $T_B$  is found to be less than 100 K and this can be due to other relaxation processes. Of particular relevance is the improvement in blocking temperature in case of **7b** compared to **7a** where all the C–H bonds of the cyclopentadienyl ring are removed intentionally. These C–H bonds are shown to be the cause of relaxation in the case of complex **7a**.

To get a deeper insight into the relaxation mechanism of these metallocenium complexes, a rigorous computational study has been performed. It was found that local molecular vibrations play an essential role in the low-temperature spin-

lattice relaxation mechanism. An approximate determination of these relaxation pathways like Raman, Orbach, Direct was already known from CASSCF-RASSI-SO methodology which takes care of the static part of the relaxation and energy states. But in-depth analysis or first principle approach on these spin-lattice relaxation dynamics has not been attempted earlier to pinpoint the under barrier relaxation in spite of showing large  $U_{\text{cal}}$  value. It was further realised from dilution experiments that local molecular vibrations (optical phonons) play a key role in determining under barrier relaxation processes. In order to solve this problem, a Master equation has been solved to obtain the spin-phonon coupling.<sup>[11c]</sup>

$$\frac{d}{dt} p_i(t) = \sum_{f \neq i} [\gamma_{fi} p_f(t) - \gamma_{if} p_i(t)] \quad (3)$$

Here  $dp/dt$  describes the changes in the population of each  $m_j$  state with respect to time and  $\gamma_{fi}$  dictates the transition rate between electronic states  $i$  and  $f$ . To calculate this, a transition matrix has been developed which constitutes of the two electronic states connected by the spin-phonon Hamiltonian. This Hamiltonian depends on the rate of change of crystal field parameters with respect to the molecular vibration or atomic displacements. Here it is to be mentioned that, not all the normal modes involve or contributes to the spin-phonon relaxation mechanism, it is those lower energy vibrations which results in a non-zero value of the transition matrix. The normal modes of vibrations arising from gas phase-frequency analysis were performed using DFT methodology on both the complexes. These computed normal modes of vibrations on the molecule also correlated with the experimentally observed IR and Raman intensities.

From the vibrational analysis, the atomic displacements were obtained as a function of time and a single point CASSCF-RASSI-SO has been performed on the structures obtained at several potential energy surface points. Next, the crystal field parameters have been plotted as a function of atomic displacements, and thus the lower energy vibrations that give a non-zero transition matrix were identified. The vibrational analysis revealed that (for complex **7a**) it was the C–H bond rocking vibrations which allow the C–H group moves towards or away from the Dy centre occurring at  $>400 \text{ cm}^{-1}$  was responsible for magnetic relaxation.<sup>[11c]</sup> Thus it was predicted that substitution of the H atoms on the Cp<sup>III</sup> ring with other R-groups would allow the magnetic relaxation to enhance the barrier further as has been seen in the case of complex **7b**. However, in complex **7b**, the C–H bond vibrations were avoided, but it was noticed that the out-of-plane vibration of Cp\* ligand at around  $640 \text{ cm}^{-1}$  causes the under barrier relaxation.<sup>[11a]</sup>

Another fascinating class of complex is reported with Dy<sup>III</sup> ion where it is sandwiched between two four-member cyclobutadiene ring, which is first of this kind, stabilized by two counter cation of K which is linked to aromatic system having molecular formula  $[\text{Dy}\{\eta^4\text{-C}_4(\text{SiMe}_3)_4\}\{\eta^4\text{-C}_4(\text{SiMe}_3)_3\text{-K}(\text{CH}_2\text{SiMe}_2)\}_2]^-$  (complex **8**) which shows an energy barrier of  $322 \text{ cm}^{-1}$  at a applied field of 1T and shows hysteresis up to

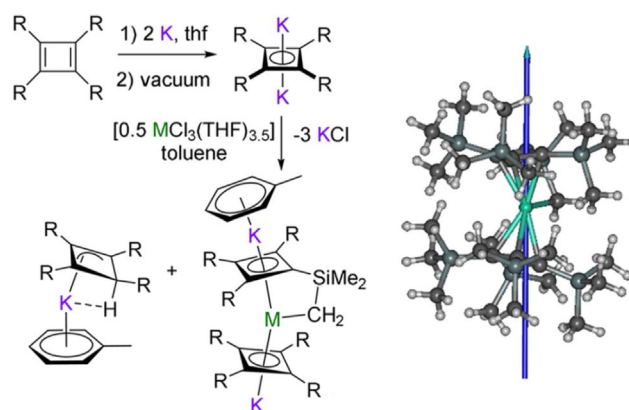


**Figure 14.** Reaction Scheme for complex **8** ( $M=\text{Dy}^{\text{III}}$ ) (left) and the ab initio computed  $g_2$  axis of the molecule at the ground state. Adapted with the permission from Ref. [38].

$7 \text{ K}$  (see Figure 14).<sup>[38]</sup> The calculated  $g$ -tensors and crystal field parameters imply the strong axially of the ground state doublet having a projection on the  $m_j = \pm 15/2$  state being close to 95%. A small-but-significant transverse component, that is,  $g_x = 0.0076$ ,  $g_y = 0.0130$ ,  $g_z = 19.7338$ , of the ground state anisotropic causes a QTM in the absence of applied dc field (see Table 2). Due to the influence of the equatorial tuck-in ligand causes substantial axial field leading to the energy splitting between the ground two levels to be at  $284 \text{ cm}^{-1}$ , which is in accord with its experimental value. There may be a significant donation of the  $\pi$  electron from the four-member to the K rather to Dy<sup>III</sup> causing a decrease of axial nature of crystal field causing field-induced SMM. The above example shows the attachment of a cation to the four-member ring causes an appreciable decrease in the  $U_{\text{eff}}$  and relaxation processes.

## 2.5. Endohedral Lanthanofullerenes as SMMs

In contrast to the above pure or pseudo organometallic magnet, these are the class of unconventional SMM with Ln<sup>III</sup> where C–Ln bond is involved but differs from the above discussed SMMs. One of the challenging aspect correlated to the organometallic lanthanide compounds is its stability under ambient conditions. As most of the complexes are unstable under ambient conditions, this renders the potential applications proposed for this molecular far-fetched. Another alternative avenue to achieve such strong donation and axially by maintaining Ln<sup>III</sup>–C bond is to encapsulate Ln<sup>III</sup> ions inside a fullerene. Several examples of this type have been reported in recent years and here we highlight the role of theoretical studies that have unearthed various such SMMs in the last few years or so. A theoretical search was undertaken to obtain very large exchange interaction between Ln-radicals lead to the suggestion of  $\text{Gd}_2@C_{79}\text{N}$  (complex **9a**) heterofullerene cages where radical tend to reside on the fullerene moiety couple with the unpaired electrons present in the Gd<sup>III</sup> ion. DFT calculations yield record high exchange of  $\approx 200 \text{ cm}^{-1}$  (using Hamiltonian  $H = -2J S_{\text{Gd}} S_{\text{rad}}$ ). Later in 2017 Hu et al. has characterised the  $\text{Gd}_2@C_{79}\text{N}$  thoroughly.<sup>[39]</sup> The high spin  $S = 15/2$  state with

a strong  $J_{\text{Gd-rad}} = 175 \pm 10 \text{ cm}^{-1}$  was experimentally verified by magnetic susceptibility measurements and additionally this molecule also shows quantum coherence (see Figure 15). Simultaneously, Popov group also looked into the magnetic characteristics of this molecule and suggested that the  $J$  values are in the range of  $170 \pm 5 \text{ cm}^{-1}$ .<sup>[40]</sup> Both are suggesting very strong ferromagnetic coupling as predicted by theory. Such a high exchange value is due to the direct interaction between the  $\text{Gd}^{\text{III}}$  and the  $\text{C}_{79}\text{N}$  radical molecule. It has been observed that there was a substantial charge transfer from the  $\text{C}_{79}\text{N}$  part to both the  $\text{Gd}^{\text{III}}$  as the HOMO of  $\text{C}_{79}\text{N}^{\cdot-}$  was low-lying in energy, which was reflected at the spin density of the  $\text{Gd}^{\text{III}}$  atoms. The spin density plot reveals that the unpaired electron lies between two  $\text{Gd}^{\text{III}}$  ions inside the cage rather than delocalised.

Replacing the isotopic Gd with strongly anisotropic Dy brings the extraordinary result in the magnetic blocking barrier value with significant quenching of QTM due to strong magnetic coupling.<sup>[41]</sup> The  $\text{Dy}_2@C_{79}\text{N}$  (complex **9b**) taken into the CASSCF + RASSI-SO/SINGLE-ANISO/POLY-ANISO module to calculate the energy blockade for magnetic reversal and it shows an energy barrier of 837.6 and  $785.7 \text{ cm}^{-1}$  at individual Dy centres with Ising type anisotropy at the ground state which is of

pure 15/2 type (see Table 2 also). Several models were taken into account as Dy-rad, Dy inside non-radical fullerene, Dy-Dy full fullerene and a various range of  $U_{\text{cal}}$  134  $\text{cm}^{-1}$  to 713  $\text{cm}^{-1}$  has been obtained which confirms as the exchange between the Dy and radical increases the  $U_{\text{cal}}$  effectively (Table 3).<sup>[42]</sup>

After this Popov and co-workers synthesised analogues complex  $\text{Dy}_2@C_{80}(\text{CH}_2\text{Ph})$  with a radical trapped in between the two Dy centres showing the blocking temperature of 18 K and  $U_{\text{eff}}$  value of 613 K ( $426 \text{ cm}^{-1}$ ) agreeing quite close to theoretical predictions.<sup>[43]</sup>

In the next phase of the fullerene type SMMs, other models focusing on the  $\text{Dy}^{\text{III}}$  ion within  $\text{C}_{72}$  (**9c**),  $\text{C}_{76}$  (**9d**) and  $\text{C}_{82}$  (**9e**) cages where the Dy-C distance estimated in the range of 2.4 to 2.6 Å and the  $\text{Dy}^{\text{III}}$  ion is bridged to the  $\text{Sc}^{\text{III}}$  ion via an oxo bridge inside the fullerene cages have been explored.<sup>[29b]</sup> The knowledge behind such an approach is that the metal atom  $\text{Sc}^{\text{III}}$  being a diamagnetic element helps to avoid weak exchange coupling between the lanthanide centres, which generally leads to close-lying excited states and faster relaxation. Another point to note is that the diamagnetic  $\text{Sc}^{\text{III}}$  ion led to significant negative charge on the oxo atom that is coordinated to the  $\text{Ln}^{\text{III}}$ , leading to strong donation and hence higher energy barrier. Additionally, among several models tested

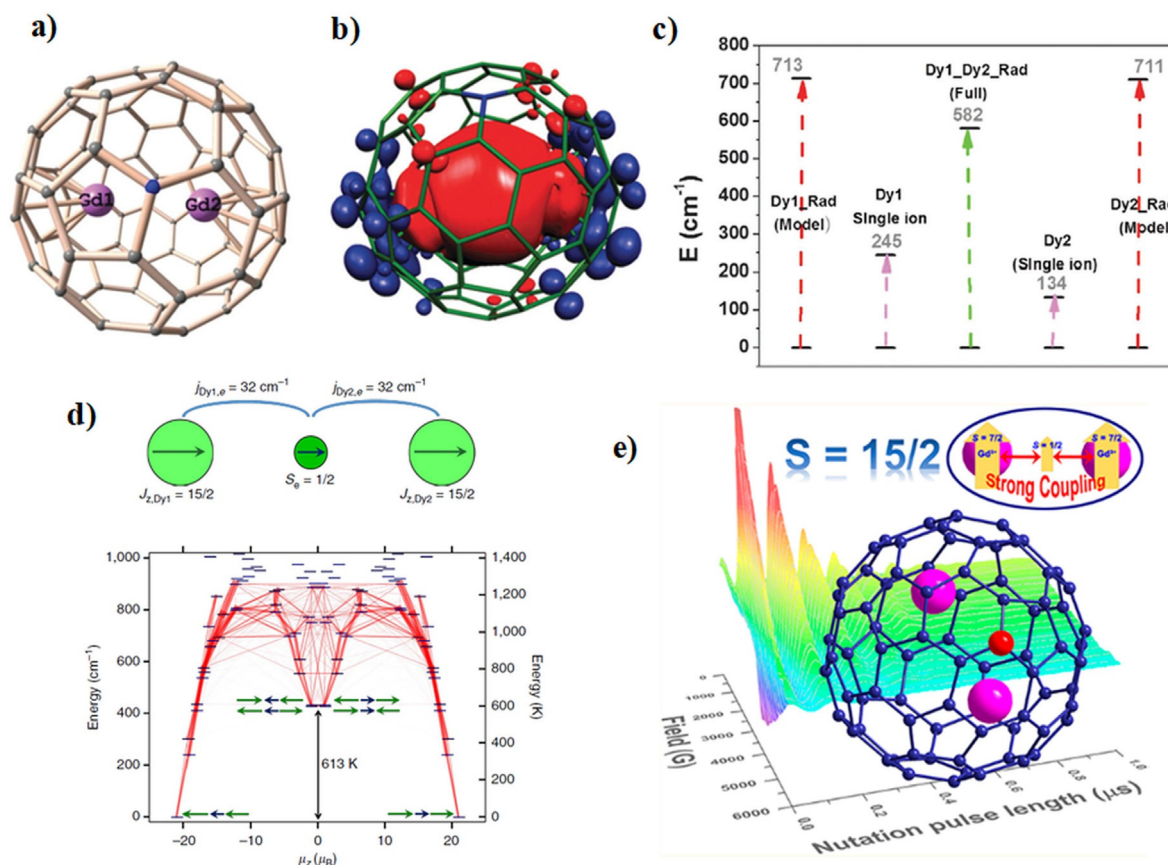


**Figure 15.** (a) DFT optimized structure of the  $\text{Gd}_2@665\text{-C}_{79}\text{N}$  isomer along with (b) its spin density plot for the  $S = 15/2$  state. (c) Diagrammatic comparison of barrier heights ( $U_{\text{cal}}$  values) estimated for different models studied for the  $\text{Dy}_2@665\text{-C}_{79}\text{N}$  molecule. (d) Schematic description of the magnetic coupling of the two  $\text{Dy}^{\text{III}}$  and the radical at ground state and project barrier height and transition probabilities with respect to  $z$ -component of the magnetic moment of the Dy-radical-Dy molecule. (e) A representative diagram of Rabi oscillation plot,  $\text{Gd}_2@C_{79}\text{N}$  molecule showing a  $S = 15/2$  ground state. All the figures are adapted with the permission from Ref. [29b,39,42,43].

**Table 3.** CASSCF+RASSI-SO computed relative energies of eight low lying KDs and g tensors of eight low lying KDs for DyOLu@C<sub>72</sub>, DyOLu@C<sub>76-1</sub> and DyOLu@C<sub>82</sub> molecules, along with deviations from the principal magnetization axes of the first KD.

M	DyOLu@C <sub>72</sub>			DyOLu@C <sub>76-1</sub>			DyOLu@C <sub>82</sub>		
	E [cm <sup>-1</sup> ]	g <sub>x</sub> , g <sub>y</sub> , g <sub>z</sub>	[°]	E [cm <sup>-1</sup> ]	g <sub>x</sub> , g <sub>y</sub> , g <sub>z</sub>	[°]	E [cm <sup>-1</sup> ]	g <sub>x</sub> , g <sub>y</sub> , g <sub>z</sub>	[°]
1	0.0	0.000, 0.000, 19.970		0.0	0.000, 0.000, 19.980		0.0	0.000, 0.000, 19.982	
2	451.6	0.006, 0.006, 17.089	4.6	396.7	0.001, 0.001, 17.139	5.1	475.2	0.001, 0.001, 17.028	2.0 1.7
3	868.6	0.037, 0.042, 14.280	7.4	790.2	0.006, 0.007, 14.293	4.7	896.1	0.029, 0.036, 14.126	1.9 2.5
4	1194.5	0.339, 0.398, 11.410	4.2	1112.2	0.080, 0.093, 11.595	1.5	1220.3	0.158, 0.194, 11.326	4.5 5.6
5	1375.5	3.852, 4.746, 7.632	16.9	1312.4	1.680, 1.869, 9.041	11.6	1430.3	0.436, 0.605, 8.486	6.2 23.9
6	1444.3	1.333, 2.344, 9.237	96.6	1385.3	2.434, 3.624, 15.367	102.3	1533.1	6.130, 6.022, 4.113	166.4 64.6
7	1470.2	0.830, 4.592, 11.085	79.5	1421.5	0.735, 3.572, 12.438	84.3	1578.8	0.012, 1.308, 14.940	84.6 75.6
8	1516.0	0.627, 1.245, 16.452	88.6	1475.4	0.663, 2.687, 17.573	87.9	1615.7	0.266, 2.198, 17.348	90.1 16.1

where coordination of the ethylene to Dy<sup>III</sup>, η<sup>2</sup> and η<sup>6</sup> coordination of benzene ring to Dy<sup>III</sup> are attempted and among all the models, the model where ethylene bridging Dy<sup>III</sup> yield large theoretical barrier height and this is followed by η<sup>2</sup> coordination of the benzene ring. This suggests that strong point charged axial donations are superior compared to delocalized donations such as the one seen in η<sup>6</sup> coordination of benzene (see Figure 16). Furthermore, the same group in 2017 also verified the large crystal field splitting in those mixed-metal Dy-Sc cluster fullerenes which were close to the models predicted earlier.<sup>[44]</sup> Additionally, sulphur analogues of Dy<sub>2</sub>O@C<sub>82</sub> like Dy<sub>2</sub>S@C<sub>82</sub>-Cs and Dy<sub>2</sub>S@C<sub>82</sub>-C<sub>3v</sub> have been synthesised and characterised using DC and AC magnetometry, and ab initio calculations and these found to exhibit attractive SMM characteristics. Most recently, Tb<sup>III</sup><sub>2</sub>@C<sub>79</sub>N has been synthesised as well and this also found to have a large blocking temperature of 15 K with the U<sub>eff</sub> value touching 526 cm<sup>-1</sup>.<sup>[45]</sup>

Another important step forward is retaining the properties of these SIMs on surfaces. There are many examples of SMMs

where the properties are lost upon adsorption. Theoretical studies play an important role in elucidating the atomistic structure of molecules adsorbed on the surface and provide insight into the nature of magnetic coupling and anisotropy.<sup>[46]</sup> A non-organometallic lanthanide compound [Er(trensal)] has been deposited in various metallic surfaces such as Au(111) and Ni thin film on Cu(100). Both experiments and theoretical studies based on periodic density functional methods offer ways to rationalise the observed strong exchange coupling between Ni-Er centres.<sup>[47]</sup> Ab initio calculations on Lanthanide SMMs on surfaces are rare at present.

### 3.1. Summary and Outlook:

In this mini-review, we have attempted to briefly review the state-of-the-art reports on the organometallic Lanthanide SIMs which are gaining significant attention in recent years. Our focus particularly pertains to the role of ab initio calculation in the design and development of SMMs based on organometallic ligands. The most important learning outcomes from this review are summarised below.

To begin with, we have shown how important is the Ln<sup>III</sup>-carbon bonds and how they are different when you have a neutral carbene type ligands interaction vis-à-vis a negative charged anionic carbon centre binding to Ln<sup>III</sup>. A significant enhancement to the crystal field splitting and thus the anisotropy obtained upon a negatively charged carbon donor ligands binding to Ln<sup>III</sup> suggests that such ligand has the potential to unravel novel molecules. Coincidentally, the substitute cyclopentadienyl ligands are similar to the stated examples, illustrating what one can achieve with organometallic Ln<sup>III</sup> compounds. Additionally, we have discussed how the carbon donor ligand can be essential to obtain SMM behaviour even when the geometries are not favourable compared to traditional N-donor ligands using pyrazolyl vs. imidazolyl moieties.

Secondly, we have discussed various lanthanoarene complexes and emphasized how important it is to choose the right Ln<sup>III</sup> ion for the right ligand architecture. Arene ligands are certainly the superstar in this area yield the best Dy<sup>III</sup> and Er<sup>III</sup> SIMs that are reported so far. From moving to main group oxo and nitro donor ligand to C donor cyclo arene type ligand can help in achieving the pseudo-linear type geometry which is most suitable for U<sub>eff</sub> enhancement of SMM. Among the hetero ligands binding to Er<sup>III</sup> along with COT<sup>2-</sup>, such as N-donor, O-donor and halides donor, iodide found to reduce the barrier significantly. The sandwich coordination of COT<sup>2-</sup> was found to be superior to any other ring coordination for Er<sup>III</sup> ion and [Er(COT)<sub>2</sub>]<sup>-</sup> is reported to be the best SIM reported for any Er<sup>III</sup>

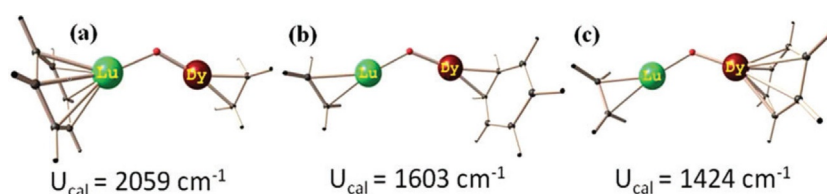


**Figure 16.** Core model for complex **9c** (a), **9d** (b) and **9e** (c) and their reported U<sub>cal</sub> values. Adapted with the permission from Ref. [28b].



till date. Contrarily,  $\text{COT}^{2-}$  was found not suitable for oblate ion  $\text{Dy}^{\text{III}}$  ion. The cyclopentadienyl  $\text{Cp}^-$  however, found to yield strong axial ligation as desired for  $\text{Dy}^{\text{III}}$  and mimic the pseudo-linear coordination. Thus  $[\text{Dy}(\text{Cp}^{\text{III}})_2]^+$  and  $[(\text{Cp}^{\text{IPr5}})\text{Dy}(\text{Cp}^*)]^+$  showed record-breaking performance in the history of lanthanocene complexes with a hysteresis opening at 60 K and 80 K respectively. The later complex was shown to possess a more towering barrier height because of lack ring C–H bonds in the Cp ring, which was predicted from the first principle vibrational study to cause relaxation at lower temperatures.

Additionally, the next generation endohedral metallofullerenes (EMF) containing paramagnetic  $\text{Ln}^{\text{III}}$  ions were discussed in the last which showed some path-breaking magnetic properties for  $\text{Gd}_2@\text{C}_{79}\text{N}$  and  $\text{Dy}_2@\text{C}_{80}(\text{CH}_2\text{Ph})$  radical fullerene molecule exhibiting very strong magnetic exchange and very large blocking temperatures. These systems have several advantages over conventional coordination/organometallic lanthanide molecule, as it is entirely possible to make molecules with any nuclear spins—one of the hard to meet criteria in this area.

### 3.1. Future directions

Here we intend to describe some future directions of ab initio methods and its limitations. One of the main challenges in CASSCF methodology is the restriction of the reference space employed. While several ways have been proposed to enhance the active space beyond (14,14) limit, there are not enough studies to see how such expansion improves the accuracy and how important is it to include dynamic correlation more beyond second-order perturbation methods. Methods such as density matrix renormalization group (DMRG or DMRG-PT2) or multi-reference coupled-cluster (MR-CCSD(T)) are actively developed and getting tested rigorously, though not at this front yet. While these methods are superior compared to the methodology that has been used, they are also computationally expensive and performing calculations using these methods without compromising the ligand architecture is a great challenge. Secondly, solving the master equation has been shown to yield mechanistic insights that are deeper than the static picture described; however, there are still several open questions. Particularly, computing accurately the vibrational levels and performing calculations at each geometric points is a tedious task and impossible for large molecules. Alternative ways to identify vibrations that are likely to trigger the relaxation needs to be developed to aid further improvement to the existing models. If this is achieved, one can perceive to calculate the blocking temperature of the SIMs directly using ab initio methods and such development, when happens, likely to result in a new way of doing this research whereby computation of spin Hamiltonian parameters will be the first step in the design and development of the desired molecules.

To this end, it is important to note that the accuracy of multi-configurational CASSCF based methods has been known for a very long time, its adaptability to Lanthanides complexes to study its degenerate states found to yield encouraging results, where these calculations reproduce well many of the ex-

perimental observables. Prior to this, the major aim of theoretician working in this area was to reproduce the experimental results and rationalise the observations often using DFT methods, which lacks rigorous predictive power. The theoretical development towards the application of such robust theory to practical molecules thoroughly revamped the area where the experimentalists begin to design experiments to validate the calculated parameters and target molecules that are predicted to possess desired magnetic characteristics. While significant breakthroughs are already witnessed, we are confident that also in the future, ab initio calculations will have their mark on next-generation SIMs that would fulfil all the criteria to be used to construct the devices desired.

### Acknowledgements

G.R. would like to acknowledge the financial support from SERB-DST (CRG/2018/000430) India. A.S. and A.S. would like to thank UGC and CSIR for an SRF fellowship, respectively.

### Conflict of interest

The authors declare no conflict of interest.

**Keywords:** Ab initio Calculations • Lanthanide SMMs • Mechanism of Magnetic relaxations • Organometallic SMMs • Single-Molecule Magnets

- [1] K. Katoh, H. Isshiki, T. Komeda, M. Yamashita, *Coord. Chem. Rev.* **2011**, 255, 2124–2148.
- [2] R. Vincent, S. Klyatskaya, M. Ruben, W. Wernsdorfer, F. Balestro, *Nature* **2012**, 488, 357.
- [3] a) R. Sessoli, D. Gatteschi, A. Caneschi, M. Novak, *Nature* **1993**, 365, 141; b) D. Gatteschi, R. Sessoli, J. Villain, *Molecular nanomagnets*, Vol. 5, Oxford University Press on Demand, Oxford, **2006**; c) D. N. Woodruff, R. E. Winpenny, R. A. Layfield, *Chem. Rev.* **2013**, 113, 5110–5148; d) C. Benelli, D. Gatteschi, *Introduction to molecular magnetism: From transition metals to lanthanides*, Wiley, New York, **2015**.
- [4] a) D. Gatteschi, *Adv. Mater.* **1994**, 6, 635–645; b) M. N. Leuenberger, D. Loss, *Nature* **2001**, 410, 789; c) A. Candini, S. Klyatskaya, M. Ruben, W. Wernsdorfer, M. Affronte, *Nano Lett.* **2011**, 11, 2634–2639; d) M. D. C. Giménez-López, F. Moro, A. La Torre, C. J. Gómez-García, P. D. Brown, J. Van Slageren, A. N. Khlobystov, *Nat. Commun.* **2011**, 2, 407.
- [5] a) A. K. Bar, P. Kalita, M. K. Singh, G. Rajaraman, V. Chandrasekhar, *Coord. Chem. Rev.* **2018**, 367, 163–216; b) M. Nakano, H. Oshio, *Chem. Soc. Rev.* **2011**, 40, 3239–3248; c) R. Sessoli, A. K. Powell, *Coord. Chem. Rev.* **2009**, 253, 2328–2341; d) G. Karotsis, S. Kennedy, S. J. Teat, C. M. Beavers, D. A. Fowler, J. J. Morales, M. Evangelisti, S. J. Dalgarno, E. K. Brechin, *J. Am. Chem. Soc.* **2010**, 132, 12983–12990; e) N. Ishikawa, Y. Mizuno, S. Takamatsu, T. Ishikawa, S.-Y. Koshihara, *Inorg. Chem.* **2008**, 47, 10217–10219.
- [6] N. Ishikawa, M. Sugita, T. Ishikawa, S.-Y. Koshihara, Y. Kaizu, *J. Am. Chem. Soc.* **2003**, 125, 8694–8695.
- [7] J. D. Rinehart, J. R. Long, *Chem. Sci.* **2011**, 2, 2078.
- [8] Z. Zhu, M. Guo, X.-L. Li, J. Tang, *Coord. Chem. Rev.* **2019**, 378, 350–364.
- [9] S. T. Liddle, J. van Slageren, *Chem. Soc. Rev.* **2015**, 44, 6655–6669.
- [10] a) R. A. Layfield, J. J. McDouall, S. A. Sulway, F. Tuna, D. Collison, R. E. Winpenny, *Chem. Eur. J.* **2010**, 16, 4442–4446; b) W. J. Evans, *Organometallics* **2016**, 35, 3088–3100; c) B. M. Day, F.-S. Guo, R. A. Layfield, *Acc. Chem. Res.* **2018**, 51, 1880–1889.
- [11] a) F.-S. Guo, B. M. Day, Y.-C. Chen, M.-L. Tong, A. Mansikkamäki, R. A. Layfield, *Science* **2018**, 362, 1400–1403; b) F. S. Guo, B. M. Day, Y. C. Chen, M. L. Tong, A. Mansikkamäki, R. A. Layfield, *Angew. Chem. Int. Ed.* **2017**,

- 56, 11445–11449; *Angew. Chem.* **2017**, *129*, 11603–11607; c) C. A. P. Goodwin, F. Ortu, D. Reta, N. F. Chilton, D. P. Mills, *Nature* **2017**, *548*, 439–442; d) K. R. McClain, C. A. Gould, K. Chakarawet, S. J. Teat, T. J. Groshens, J. R. Long, B. G. Harvey, *Chem. Sci.* **2018**, *9*, 8492–8503.
- [12] a) J. R. M. Long, A. O. Tolpygin, A. V. Cherkasov, K. A. Lyssenko, Y. Guari, J. Larionova, A. A. Trifonov, *Organometallics* **2019**, *38*, 748–752; b) L. Escalera-Moreno, J. J. Baldoví, A. Gaita-Ariño, E. Coronado, *Inorg. Chem.* **2019**, *58*, 11883–11892.
- [13] J. Lu, M. Guo, J. Tang, *Chem. Asian J.* **2017**, *12*, 2772–2779.
- [14] a) J.-L. Liu, Y.-C. Chen, Y.-Z. Zheng, W.-Q. Lin, L. Ungur, W. Wernsdorfer, L. F. Chibotaru, M.-L. Tong, *Chem. Sci.* **2013**, *4*, 3310–3316; b) J. Tang, I. Hewitt, N. T. Madhu, G. Chastanet, W. Wernsdorfer, C. E. Anson, C. Benelli, R. Sessoli, A. K. Powell, *Angew. Chem. Int. Ed.* **2006**, *45*, 1729–1733; *Angew. Chem.* **2006**, *118*, 1761–1765; c) L. F. Chibotaru, L. Ungur, A. Soncini, *Angew. Chem. Int. Ed.* **2008**, *47*, 4126–4129; *Angew. Chem.* **2008**, *120*, 4194–4197.
- [15] L. Ungur in *Lanthanide-Based Multifunctional Materials*, Elsevier, Amsterdam, **2018**, pp. 1–58.
- [16] C. Rudowicz, *J. Phys. C* **1985**, *18*, 1415.
- [17] R. A. Layfield, *Organometallics* **2014**, *33*, 1084–1099.
- [18] R. Marx, F. Moro, M. Dörfel, L. Ungur, M. Waters, S.-D. Jiang, M. Orlita, J. Taylor, W. Frey, L. Chibotaru, *Chem. Sci.* **2014**, *5*, 3287–3293.
- [19] F. T. Edelmann, *Coord. Chem. Rev.* **2017**, *338*, 27–140.
- [20] S. G. McAdams, A.-M. Ariciu, A. K. Kostopoulos, J. P. Walsh, F. Tuna, *Coord. Chem. Rev.* **2017**, *346*, 216–239.
- [21] S. K. Singh, T. Gupta, L. Ungur, G. Rajaraman, *Chem. Eur. J.* **2015**, *21*, 13812–13819.
- [22] L. F. Chibotaru, L. Ungur, *J. Chem. Phys.* **2012**, *137*, 064112.
- [23] K. Stevens, *Proc. Phys. Soc. Sect. A* **1952**, *65*, 209.
- [24] C. A. Rudowicz, *J. Chem. Phys.* **1986**, *84*, 5045–5058.
- [25] C. Rudowicz, M. Karbowiak, *Coord. Chem. Rev.* **2015**, *287*, 28–63.
- [26] S. K. Gupta, T. Rajeshkumar, G. Rajaraman, R. Murugavel, *Chem. Sci.* **2016**, *7*, 5181–5191.
- [27] L. Ungur, L. F. Chibotaru, *Inorg. Chem.* **2016**, *55*, 10043–10056.
- [28] J.-L. Liu, Y.-C. Chen, M.-L. Tong, *Chem. Soc. Rev.* **2018**, *47*, 2431–2453.
- [29] a) T. Gupta, G. Velmurugan, T. Rajeshkumar, G. Rajaraman, *J. Chem. Sci.* **2016**, *128*, 1615–1630; b) M. K. Singh, G. Rajaraman, *Chem. Commun.* **2016**, *52*, 14047–14050.
- [30] R. Note, These models are optimised within DFT framework B3LYP/CSDZ(GD), SVP(rest) and subjected to CASSCF/RASSI-SO/SINGLE\_ANISO calculations.
- [31] T. Gupta, G. Rajaraman, *Eur. J. Inorg. Chem.* **2018**, 3402–3412.
- [32] Y.-N. Guo, L. Ungur, G. E. Granroth, A. K. Powell, C. Wu, S. E. Nagler, J. Tang, L. F. Chibotaru, D. Cui, *Sci. Rep.* **2014**, *4*, 5471.
- [33] M. Gregson, N. F. Chilton, A.-M. Ariciu, F. Tuna, I. F. Crowe, W. Lewis, A. J. Blake, D. Collison, E. J. McInnes, R. E. Winpenny, *Chem. Sci.* **2016**, *7*, 155–165.
- [34] J. D. Hilgar, M. G. Bernbeck, B. S. Flores, J. D. Rinehart, *Chem. Sci.* **2018**, *9*, 7204–7209.
- [35] L. Ungur, J. J. Le Roy, I. Korobkov, M. Murugesu, L. F. Chibotaru, *Angew. Chem. Int. Ed.* **2014**, *53*, 4413–4417; *Angew. Chem.* **2014**, *126*, 4502–4506.
- [36] S. K. Singh, T. Gupta, G. Rajaraman, *Inorg. Chem.* **2014**, *53*, 10835–10845.
- [37] F. Gendron, B. Pritchard, H. Bolvin, J. Autschbach, *Dalton Trans.* **2015**, *44*, 19886–19900.
- [38] B. M. Day, F. S. Guo, S. R. Giblin, A. Sekiguchi, A. Mansikkamaki, R. A. Layfield, *Chem. Eur. J.* **2018**, *24*, 16779–16782.
- [39] Z. Hu, B.-W. Dong, Z. Liu, J.-J. Liu, J. Su, C. Yu, J. Xiong, D.-E. Shi, Y. Wang, B.-W. Wang, *J. Am. Chem. Soc.* **2018**, *140*, 1123–1130.
- [40] G. Velkos, D. Krylov, K. Kirkpatrick, X. Liu, L. Spree, A. Wolter, B. Büchner, H. Dorn, A. Popov, *Chem. Commun.* **2018**, *54*, 2902–2905.
- [41] a) L. J. Wilson, D. W. Cagle, T. P. Thrash, S. J. Kennel, S. Mirzadeh, J. M. Alford, G. J. Ehrhardt, *Coord. Chem. Rev.* **1999**, *190*, 199–207; b) W. Fu, J. Zhang, T. Fuhrer, H. Champion, K. Furukawa, T. Kato, J. E. Mahaney, B. G. Burke, K. A. Williams, K. Walker, *J. Am. Chem. Soc.* **2011**, *133*, 9741–9750; c) T. Zuo, L. Xu, C. M. Beavers, M. M. Olmstead, W. Fu, T. D. Crawford, A. L. Balch, H. C. Dorn, *J. Am. Chem. Soc.* **2008**, *130*, 12992–12997.
- [42] M. K. Singh, N. Yadav, G. Rajaraman, *Chem. Commun.* **2015**, *51*, 17732–17735.
- [43] F. Liu, D. S. Krylov, L. Spree, S. M. Avdoshenko, N. A. Samoylova, M. Rosenkranz, A. Kostanyan, T. Greber, A. U. Wolter, B. Büchner, *Nat. Commun.* **2017**, *8*, 16098.
- [44] a) C.-H. Chen, D. S. Krylov, S. M. Avdoshenko, F. Liu, L. Spree, R. Yadav, A. Alvertis, L. Hozoi, K. Nenkov, A. Kostanyan, *Chem. Sci.* **2017**, *8*, 6451–6465; b) D. Krylov, F. Liu, S. Avdoshenko, L. Spree, B. Weise, A. Waske, A. Wolter, B. Büchner, A. Popov, *Chem. Commun.* **2017**, *53*, 7901–7904.
- [45] A. A. Popov, G. Velkos, D. Krylov, K. Kirkpatrick, L. Spree, V. Dubrovin, B. Büchner, S. Avdoshenko, V. Bezmelnitsyn, S. Davis, P. Faust, J. Duchamp, H. C. Dorn, A. A. Popov, *Angew. Chem. Int. Ed.* **2019**, *58*, 5891–5896; *Angew. Chem.* **2019**, *131*, 5951–5956.
- [46] a) M. Mannini, F. Pineider, P. Sainctavit, C. Danieli, E. Otero, C. Sciancalepore, A. M. Talarico, M.-A. Arrio, A. Cornia, D. Gatteschi, *Nat. Mater.* **2009**, *8*, 194; b) F. Totti, G. Rajaraman, M. Iannuzzi, R. Sessoli, *J. Phys. Chem. C* **2013**, *117*, 7186–7190; c) R. Nabi, G. Rajaraman, *Chem. Commun.* **2019**, *55*, 8238–8241.
- [47] J. Dreiser, C. Wäckerlin, M. E. Ali, C. Piamonteze, F. Donati, A. Singha, K. S. Pedersen, S. Rusponi, J. Bendix, P. M. Oppeneer, *ACS Nano* **2014**, *8*, 4662–4671.

Manuscript received: June 18, 2019

Revised manuscript received: September 23, 2019

Accepted manuscript online: September 26, 2019

Version of record online: October 24, 2019